Deliverable Report

Deliverable No: D1.4

Deliverable Title: High quality q-plates with new geometries, tunability, radial-mode corrections

Grant Agreement number: 255914

Project acronym: PHORBITECH

Project title: A Toolbox for Photon Orbital Angular Momentum Technology

Project website address: www.phorbitech.eu

Name, title and organization of the scientific representative of deliverable's lead beneficiary (task leader):

Prof. Lorenzo Marrucci

Università di Napoli Federico II (UNINA)

Naples, Italy

Deliverable table

Deliverable no.	D1.4
Deliverable name	High quality q-plates with new geometries, tunability, radial-mode corrections
WP no.	1
Lead beneficiary no.	3 (ICFO)
Nature	P, R
Dissemination level	PU
Delivery date from Annex I	Month 18
Actual delivery date	31 March 2012

D1.4) Novel q-plates: *High quality q-plates with new geometries, tunability, radial-mode corrections[Excerpt from GA-Annex I DoW]*

Excerpt from Annex I: This task is aimed at designing and manufacturing novel kinds of q-plates. The q-plate is a device invented in Naples (UNAP) that introduces an interaction of polarization and OAM degrees of freedom. It may be used in particular for controlling an OAM variation with the input polarization of an optical beam, thus enabling an OAM beam generation from a Gaussian input. The basic concept of the q-plate is simply that of suitably patterned birefringent wave-plates where the coupling with the wavefront arises from the geometrical Pancharatnam-Berry phase occurring in the optical polarization manipulations. Patterned wave-plates for the visible or near IR domain can be conveniently developed using liquid crystals technology. To obtain OAM states, the pattern must have a singularity of charge q at its center, allowing for the generation of OAM states with index m = ±2q, where the sign is determined by the input circular polarization content. Only specific simple patterns having circular symmetry have been realized so far (corresponding to q=1), but technologies for realizing arbitrary patterns do exist. Another issue is the tunability of the q-plate, corresponding to the control of the wave-plate overall birefringence retardation at a given wavelength. This task is organized into two sub-tasks put in series, which will be carried out in close collaboration between UNAP (designing and manufacturing q-plates and q-plate-based optical systems and testing their performances in the classical regime) and UROM (testing the same devices in the quantum regime).

Subtask T1.2.1 – Novel q-plate development and quality improvement.

Different approaches to higher-quality and more flexible patterning (holographic, UV masking, micro-rubbing, laser writing) will be considered and tested. Mechanical and electrical tuning will also be developed (presently only thermal tuning has been demonstrated). The goal will be that of producing q-plates with arbitrary q values and controlled birefringent retardation. In addition, tailoring of the generated radial mode will be also pursued with the goal of obtaining propagation-stable superpositions of different OAM modes (the idea here is the same as that given for the holographic approach, see Task WP1.1). UROM will characterize the quality of the q-plates developed by UNAP in the quantum few-photon regime, by exploiting the experimental and theoretical tools developed for the reconstruction of quantum transformations, very sensitive to the mode purity. The goal will be to optimize the conversion efficiency, quality of the mode generated, the wavelength tuning in the quantum regime of the device. The results of this subtask will be assessed at milestone MS6 and provide a necessary input to task WP2.2.

The sub-task (T1.2.1) has started at the beginning of the project and ended regularly at month 18 (Milestone MS6).

As a first step, we have developed and successfully demonstrated the electric tuning technology of q-plates [1], which guarantees a rapid switching and convenient control of the q-plate retardation. The mechanical tuning was also briefly tested, but it proved to be not sufficiently reliable so it was discarded.

Moreover, with the collaboration of a group based in Hong Kong (prof. V. Chigrinov) and specialized in manufacturing photosensitive materials, we have set up and demonstrated a first photo-induced patterning method based on blue light illumination, allowing for a more flexible patterning and leading to higher optical quality of the q-plates compared to the previous rubbing-based method. In particular, the Hong Kong group provided different photosensitive materials to be tested and advice and training in the photo-alignment procedures, while Naples group conceived the work and performed the experiments. This work has allowed the first demonstration of tunable q-plates having arbitrary topological charge q [2].

An automatic setup for q-plate manufacturing was developed in Naples. This programmable setup allows manufacturing of q-plates with arbitrary q (both integer, semi-integer and fractional) or, in principle, any other polarization pattern with angular dependence only (see, e.g., Fig. 1a). The setup can operate with both blue and UV (a He-Cd laser from VM-TIM, purchased specifically for this purpose) light source for writing. With this setup we have tested different materials, either provided by the Hong Kong group or alternative commercial ones. We have achieved UV laser writing of the q-plates, with the purpose of having more

durable high-quality devices, which can be used with laser light having a wavelength in the whole visible and near-infrared spectrum.

With this step, the research on the purely azimuthal-patterned q-plate devices as introduced in the project has been concluded, providing high quality samples with OAM conversion efficiencies ranging from 100:1 to 1000:1 (comparable to common liquid crystal devices) and central defect sizes down to a minimum of 10 µm (Fig. 2), able to operate in the whole visible spectrum and with the possibility of electrical tuning and switching. The subsequent work was devoted to finding more general useful patterns, and in particular investigating the possibility of radial patterning and even of arbitrary 2D laser writing.

A first result along this line is the following one. The q-plate manufacturing setup was used to create a new type of device, an OAM-mode converter, that can convert the impinging OAM eigenstate of order l into an equal-weight superposition of l and $-l$ OAM modes. This converter is essentially made as a q-plate of charge q divided into $2q$ equal sectors which are rotated by 90 degree with respect to each other (see Fig. 1b for an example). These LC mode converters have similar quality properties and are controlled by electric field just as standard q-plates.

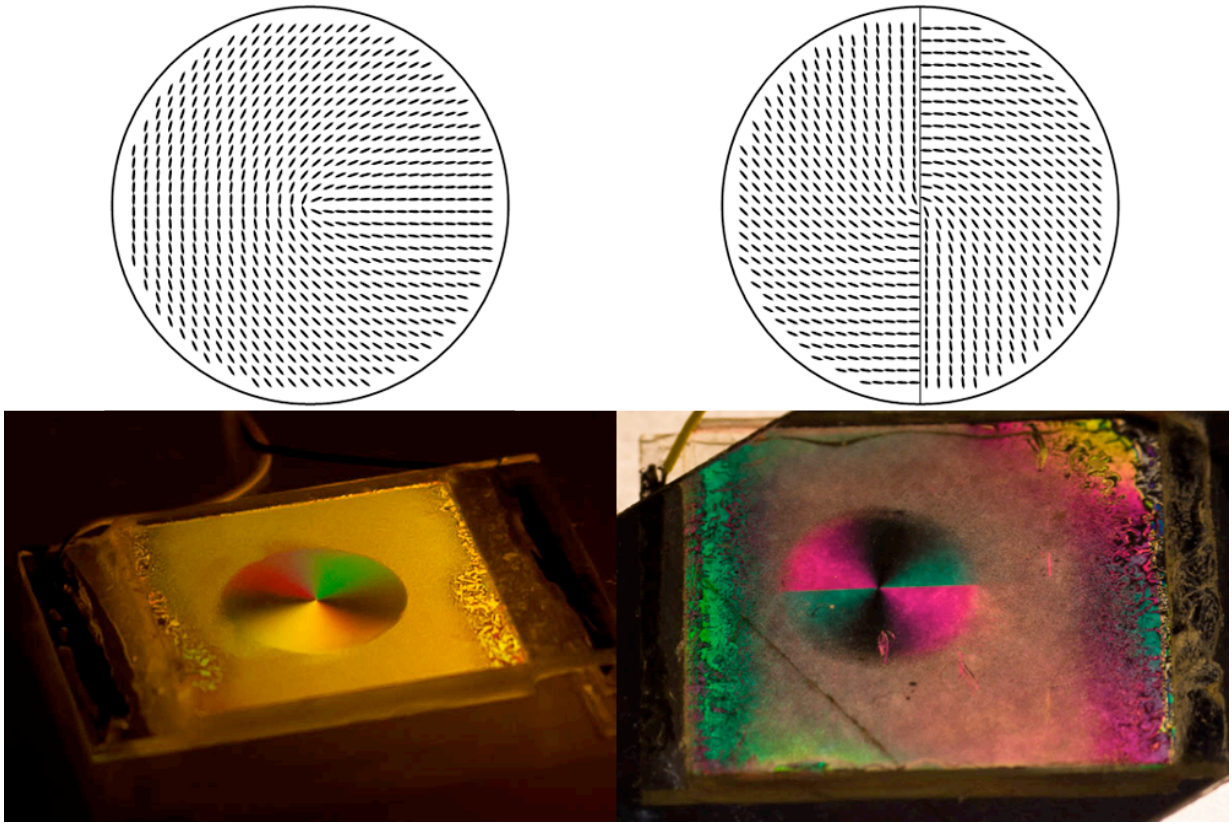

(a) **(b)**

Fig. 1 (a) a q-plate with q = 1/2, **(b)** an OAM-mode converter for $l=1$. Top row: pattern simulations. Bottom row: photos of samples placed between crossed polarizers under oblique illumination. The black fringes indicate the zones where the LC is oriented parallel to one of the polarizers and the bright zones correspond to other LC orientations. In case of the OAM-converter a disclination line in LC orientation is clearly visible under oblique illumination.

With the aim of introducing a more general patterning technology of the q-plates, another setup was developed based on a holographic approach. Essentially, this setup is based on a polarizing Mach-Zehnder interferometer that gives rise to an interference pattern between two orthogonally polarized beams. In the case of circular polarizations, no interference fringes are visible, but a linear polarization pattern is formed, depending on the wavefronts shape of two interfering beams, which can then be used to align the polymer coating of the q-plate cells so as to obtain a similar pattern of the optical axis. Such form of polarization-

holography technique allows single-step recording of different pattern structures, with both radial and azimuthal dependence. We demonstrated the capability of this setup to achieve radial patterning, by developing a liquid crystal lens (Fig. 3) based on the Pancharatnam-Berry phase, i.e. the same working principle as the q-plates (optical elements working on this principle are called Pancharatnam-Berry phase Optical Elements, or PBOEs).

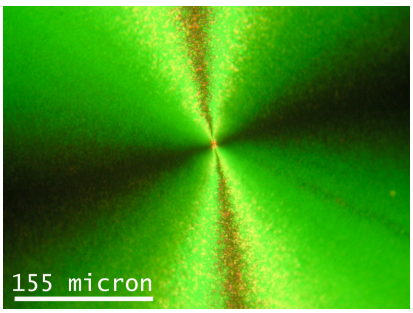

Fig. 2 - An image of a q-plate with q =1, with a central defect having a radius smaller than 10 µm.

A set of these newly produced q-plates has been made available to UROM, which has tested their performances in the quantum regime and is using them for developing novel devices for OAM control of single photons and photon pairs. Some of the results have been reported as deliverables D2.2 (deterministic transferrers) and others are still under way and will be reported in future deliverables.

In a separate work, the q-plate capability of generating vector vortex beams was studied in UNAP [3]. A q = 0.5 q-plate was used to generate azimuthally and radially polarized beams with the possibility of high-speed switching between polarization patterns by changing the impinging polarization state. More complex polarization patterns of vector beams are achievable with different topological charges of the q-plates and are currenyl beying studied.

In addition to the main line of research based on liquid crystals, we have investigated samples of silver-doped glasses under laser exposure, demonstrating that a permanent q-plate-like structure may develop spontaneously in these systems [4]. The exposure time allows control of the birefringent retardation, so that this self-patterning approach might provide an alternative approach to q-plate manufacturing in the future.

Finally, in order to assess the present status of the possible q-plate applications, a survey of the recent literature on this topic was completed and published in a review article [5], which has been also selected by the journal as one of its highlights for 2011.

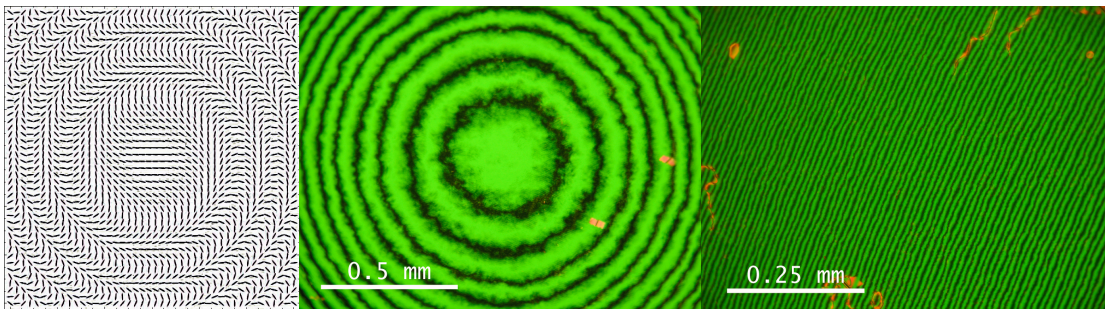

Fig. 3 (a) A pattern of a PBOE lens. **(b)** and **(c)** Lens photo under polarizing microscope, central zone and side zone respectively.

Publications included in this deliverable:

[1] "Photon spin-to-orbital angular momentum conversion via an electrically tunable q-plate", B. Piccirillo, V. D'Ambrosio, S. Slussarenko, L. Marrucci, E. Santamato, *Appl. Phys. Lett*. **97**, 241104 (2010). [NOTE: this publication has also been reported as part of deliverable D2.2]

[2] S. Slussarenko, A. Murauski, T. Du, V. Chigrinov, L. Marrucci, E. Santamato, "Tunable liquid crystal q-plates with arbitrary topological charge", *Opt. Express* **19**, 4085-4090 (2011).

[3] J. M. Amjad, H. R. Khalesifard, S. Slussarenko, E. Karimi, L. Marrucci, E. Santamato, "Laser-induced radial birefringence and spin-to-orbital optical angular momentum conversion in silver-doped glasses", *Appl. Phys. Lett.* **99**, 011113 (2011).

[4] F. Cardano, E. Karimi, S. Slussarenko, L. Marrucci, C. de Lisio, E. Santamato, "Polarization pattern of vector vortex beams generated by q-plates with different topological charges", *Appl. Opt.* **51** (10), pp. C1–C6 (2012)

[5] L. Marrucci, E. Karimi, S. Slussarenko, B. Piccirillo, E. Santamato, E. Nagali, F. Sciarrino, "Spin-to-orbital conversion of the angular momentum of light and its classical and quantum applications", *J. Opt.* **13**, 064001 (2011).

Photon spin-to-orbital angular momentum conversion via an electrically tunable *q*-plate

Bruno Piccirillo,[1,a)] Vincenzo D'Ambrosio,[1] Sergei Slussarenko,[1] Lorenzo Marrucci,[1,2] and Enrico Santamato[1]
[1]*Dipartimento di Scienze Fisiche, Università di Napoli "Federico II", Complesso Universitario di Monte S. Angelo, 80126 Napoli, Italy*
[2]*CNR-SPIN, Complesso Universitario di Monte S. Angelo, 80126 Napoli, Italy*

(Received 20 October 2010; accepted 23 November 2010; published online 16 December 2010)

Exploiting electro-optic effects in liquid crystals, we achieved real-time control of the retardation of liquid-crystal-based *q*-plates through an externally applied voltage. Electro-optic *q*-plates can be operated as electrically driven converters of photon spin into orbital angular momentum, enabling a variation of the orbital angular momentum probabilities of the output photons over a time scale of milliseconds. © *2010 American Institute of Physics*. [doi:10.1063/1.3527083]

For years the orbital angular momentum (OAM) of photons has been consigned to a back seat in the study of both classical and quantum optics. This was partly due to the conceptual reason that, in general, the spin and orbital contributions of the electromagnetic angular momentum cannot be considered separately,[1] except within the paraxial approximation. However, even in the small-angle limit, the OAM, due to the dearth of tools suitable for its manipulation, has been used much less than spin angular momentum (SAM). No doubt, the interest for both fundamental and applicative aspects of OAM has kept up with the development of methods and devices for its manipulation. At present, the importance of OAM for quantum optics is mainly due to the fact that it is defined on an infinite-dimensional Hilbert space and, by its own nature, could be suitable for implementing single-photon qudits, which may lead, for example, to simplifying quantum computations[2] and improving quantum cryptography.[3] The most commonly used methods for generating and manipulating the OAM are based on computer generated holograms (CGHs). A recently introduced tool for OAM control is a liquid-crystal-based birefringent plate with retardation δ and optical axis unevenly oriented according to a distribution with topological charge q, after which the name *q*-plate (QP).[4] A QP modifies the angular momentum state of an incident photon by giving to each of its circularly polarized components a finite probability, depending on the retardation δ, of finding the photon in a polarization state with opposite helicity and OAM quantum number l increased or decreased by the amount $\Delta l = 2q$, whether the initial helicity is positive or negative, respectively. In *q*-plates with $q = 1$, the optical axis distribution is cylindrically symmetric around the central defect and the total angular momentum of the incident photons is therefore conserved [SAM-to-OAM conversion (STOC)]. The adoption of such device in quantum optics has recently enabled the observation of two-photon Hong–Ou–Mandel coalescence interference of photons carrying nonzero OAM and the demonstration of the $1 \rightarrow 2$ universal optimal quantum cloning of OAM-encoded qubits and qudits.[5] Besides the topological charge q, a key-feature of a QP is the birefringent retardation since it enables to regulate the probability of switching between l and $l \pm 2q$, i.e., the STOC efficiency, according to the wavelength of the input photons. High efficiencies for generation, manipulation, and detection of OAM states are often desirable, especially when only few photons are available.

In this paper, to achieve a full control of the STOC efficiency, we present an electro-optical *q*-plate (EOQP) whose retardation may be changed through an externally applied voltage. Hitherto, STOC efficiencies exceeding 95% (significantly higher than the efficiencies of the CGHs) were obtained tuning the *q*-plate retardation δ by controlling the material temperature.[6] A thermally tuned QP has been used with a Dove prism inserted into a Sagnac polarizing interferometer in order to generate arbitrary linear combinations of OAM eigenstates with $l = \pm 2$ by manipulating the polarization state of an input linearly polarized TEM_{00} laser beam.[7] The thermal tunability of δ arises from the temperature dependence of the liquid crystal order parameter and ultimately of the intrinsic birefringence of such material. The thermal control of a QP assures an easy-to-made stable retardation at the cost of a very slow time response. This is a limitation whenever the experiment requires a real-time variation of STOC efficiency, for instance, for qudit manipulation or when more wavelengths are involved. Electric-field-based regulation of δ enables one to overcome the time-response limitations imposed by the thermal method and make QPs suitable for more demanding tasks. The working principle of EOQP is based on the well-known property of external static electric or magnetic fields to change the orientation of the liquid-crystal molecular director $\boldsymbol{n}$, representing the local average orientation of liquid crystal molecules.[8] We fabricated and tested two EOQPs with $q = 1$ so that the OAM impressed to converted photons is $l = \pm 2$. These devices have different thicknesses and have been manufactured by different methods. The first was a nominal 20 μm thick film of E7 liquid crystal from Merck Ltd., sandwiched between two indium-tin-oxide (ITO)-coated glass substrates, beforehand coated with a polyimide for planar alignment and circularly rubbed, as described elsewhere.[6] The second EOQP was a nominal 6 μm thick film of E7, sandwiched between two ITO-coated glass substrates, beforehand coated with a polyimide UV-photoaligned for planar topologically charged optical axis distribution. The ITO transparent conductive films work as electrodes for the application of an electric field to the liquid

a)Electronic mail: bruno.piccirillo@na.infn.it.

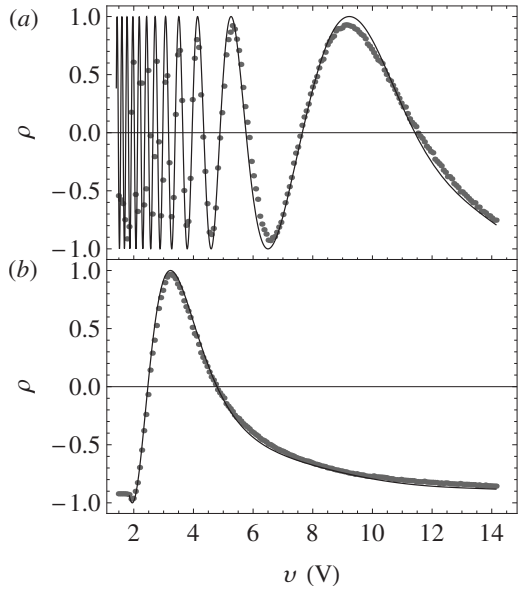

FIG. 1. Measured contrast ratio $\rho(v)=\cos\delta(v)$ reported as function of v for $EOQP_1$ (a) and $EOQP_2$ (b). The continuous lines represent the theoretical behaviors.

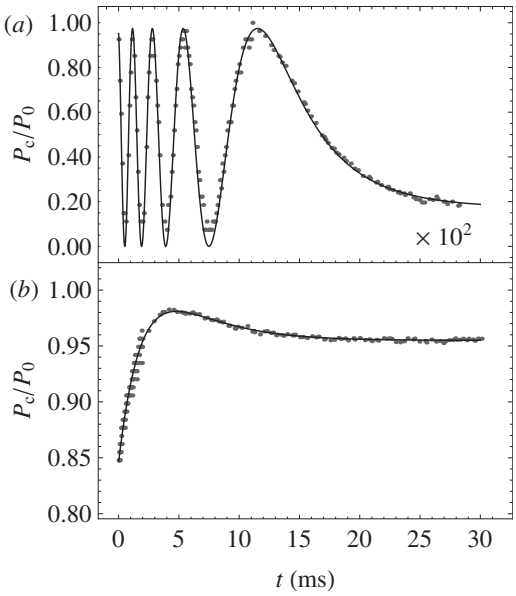

FIG. 3. Time decay of the power of the converted components of the output beam for $EOQP_1$ (a) and $EOQP_2$ (b) after the voltage switch-off. The starting voltages were $v_1=2.8$ V for $EOQP_1$ and $v_2=2.2$ V for $EOQP_2$ so that the dynamics may be approached in the small distortion limit and compared with theory (continuous lines). The time scale in panel (a) is slower by a factor of 100 with respect to panel (b).

crystal. From now on, the former device will be referred to as $EOQP_1$ and the latter as $EOQP_2$. Adopting essentially the same apparatus as that described in Ref. 6 for both the EOQPs, we measured, as a function of the applied voltage, the powers of the converted (P_c) and unconverted (P_u) components of the output beam for an incident $\lambda=532$ nm circularly polarized TEM_{00} laser beam. The temperature of both the EOQPs was maintained stable at 30 °C during measurements. P_u and P_c are expected to depend on the optical retardation δ according to the Malus-like laws,[6] $P_u=P_0\cos^2(\delta/2)$ and $P_c=P_0\sin^2(\delta/2)$, where P_0 is the total output power. In Fig. 1, the contrast ratios $\rho(v)=(P_u-P_c)/(P_u+P_c)=\cos\delta(v)$ are shown for the rubbing-aligned and UV-photoaligned EOQPs, respectively, as functions of the rms values v of the applied 1 kHz ac voltage.[9] The dependence of $\delta(v)$ on the voltage arises from the torque exerted on the liquid crystal molecules by the applied electric field.[8] The behavior of $\delta(v)$ vs v, as deduced from $\rho(v)$, is shown in Fig. 2 for both devices. For $v<v_{th}=1.85\pm0.01$ V, the nematic is undistorted in both the EOQPs and $\delta(0)=\delta_0=2\pi\Delta nL/\lambda+\delta_0^*$, where L stands for the thickness of the cell, $\Delta n=0.23$ is the intrinsic birefringence of the nematic E7 at 30 °C, and δ_0^* is a small constant residual birefringence. For $EOQP_1$, $\delta_0\approx1.7\pi$ and for $EOQP_2$, $\delta_0\approx0.8\pi$. For $v=v_{th}$ there is a discontinuity in the slope $d\delta/dv$. This is peculiar of a second order phase transition between the unperturbed and the distorted conformations at the critical voltage v_{th} (Freédericksz transition).[8] The theory of electro-optical effects in liquid crystals[8] predicts that $v_{th}=\pi\sqrt{k_{11}/\epsilon_0\epsilon_a}$, where $k_{11}=9.2\times10^{-12}$ N (30 °C) is the splay elastic constant of the liquid crystal,[10] ϵ_0 is the vacuum dielectric constant, and $\epsilon_a=14.3$ at 1 kHz at 30 °C.[11] Actually, such expression returns $v_{th}\lesssim1$ V, i.e., half the experimental value. Such disagreement could be ascribed to the underlying simplified assumption of pure splay deformation. However, consistent with the theory, the experimental values of v_{th}, within the experimental uncertainties, turn out to be the same for both EOQPs, which differ from one another in the thickness only. In the limit of high applied voltage, the overall change $\Delta=\delta_0-\delta(\infty)=\delta_0-\delta_0^*=2\pi\Delta nL/\lambda$ is $\Delta\approx56.8$ for $EOQP_1$ and $\Delta\approx6.1$ for $EOQP_2$, yielding $L\approx21$ μm for $EOQP_1$ and $L\approx2.3$ μm for $EOQP_2$, respectively.

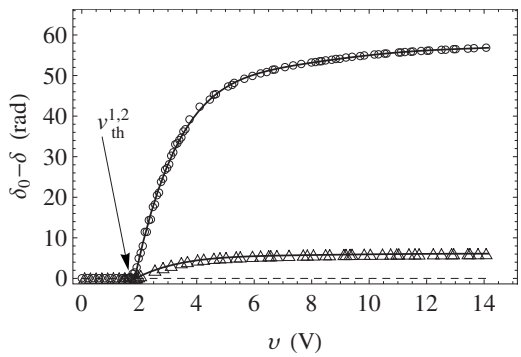

FIG. 2. The optical phase change $\delta(v)$ vs the applied voltage as extracted from the contrast $\rho(v)$ for $EOQP_1$ (○) and $EOQP_2$ (△). The continuous lines correspond to sixth order polynomial curve obtained by fitting the experimental data.

The different thicknesses of the cells are responsible for the different saturation values of $\delta(v)$ and for their different switching-off times. Assuming, for simplicity, that the initial director alignment is homogeneous, the switching-off reorientation in the small distortion limit is expected to decay exponentially in time with a constant $\tau=\gamma_1/k_{11}(L/\pi)^2$, where $\gamma_1=150$ mPa (30 °C) is the rotational viscosity of the liquid crystal.[12] The time behavior of the switching-off P_c signals is consistent with such prediction and the measured decay time constants are $\tau_1=0.931\pm0.002$ s and $\tau_2=(0.80\pm0.01)\times10^{-2}$ s, respectively (Fig. 3). These values are in reasonable agreement with those expected from theory, i.e., $\tau_1^{theor}=0.53$ s and $\tau_2^{theor}=0.62\times10^{-2}$ s. Nevertheless, consistent with the theoretical prediction for τ, $EOQP_2$, due to its reduced thickness, switches off much faster than

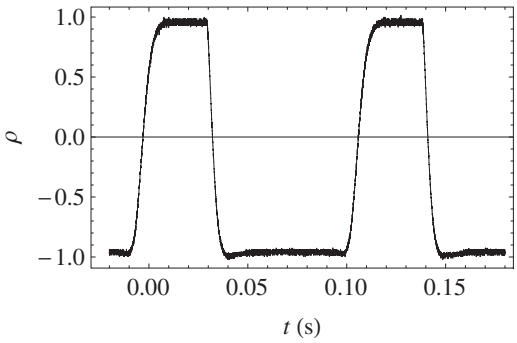

FIG. 4. Time behavior of contrast ratio ρ for on-off switching of the applied voltage (v_{on}=3.2 V) for $EOQP_2$.

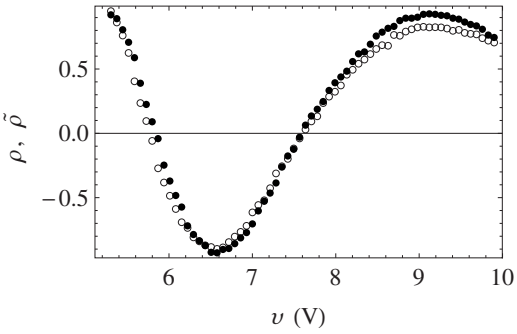

FIG. 5. Contrast ratio vs voltage for the output beam sorted with respect to polarization, $\rho(v)$, (●) and with respect to OAM, $\tilde{\rho}(v)$, (○). Data refer to $EOQP_1$.

$EOQP_1$ and may be used for fast switching between different values of δ, as shown in Fig. 4. Finally, in order to check that the EOQPs actually work as SAM-to-OAM converters, the OAM of the output beam was directly measured adopting a method of sorting between $l=0$ and $l=\pm 2$ based on a polarizing Sagnac interferometer, with a Dove prism inserted along one of its arm, as elsewhere suggested.[7] For $EOQP_1$, the contrast ratio between the OAM components of the output beam was measured as $\tilde{\rho}(v)=(P_0-P_2)/(P_0+P_2)$, where P_0 and P_2 are the powers of the $l=0$ and $l=|2|$ output components, respectively. In Fig. 5, $\tilde{\rho}(v)$ was reported, for comparison, together with $\rho(v)$, as reported in Fig. 1(a), but over a restricted voltage interval (5–10 V). The correlation between the two signals is 99.6%.

In summary we realized an electro-optical SAM-to-OAM converter aimed not only at improving the handiness of classical QPs but also at performing unusual tasks exploiting the capability of EOQPs of managing superpositions of OAM eigenstates with $l=0$, $l=2$, and $l=-2$ in real-time for high-dimensional qudits' manipulation.

We acknowledge the financial support of the FET-Open Program within the Seventh Framework Programme of the European Commission under Grant No. 255914—Phorbitech.

[1] J. D. Jackson, *Classical Electrodynamics* (Wiley, New York, 1989).
[2] A. Muthukrishnan and C. R. Stroud, Jr., Phys. Rev. A **62**, 052309 (2000); B. P. Lanyon, M. Barbieri, M. P. Almeida, T. Jennewein, T. C. Ralph, K. J. Resch, G. J. Pryde, J. L. O'Brien, A. Gilchrist, and A. G. White, Nat. Phys. **5**, 134 (2009).
[3] I. Bregman, D. Aharonov, M. Ben-Or, and H. S. Eisenberg, Phys. Rev. A **77**, 050301 (2008).
[4] L. Marrucci, C. Manzo, and D. Paparo, Phys. Rev. Lett. **96**, 163905 (2006).
[5] E. Nagali, F. Sciarrino, F. D. Martini, L. Marrucci, B. Piccirillo, E. Karimi, and E. Santamato, Phys. Rev. Lett. **103**, 013601 (2009); E. Nagali, L. Sansoni, F. Sciarrino, F. D. Martini, L. Marrucci, B. Piccirillo, E. Karimi, and E. Santamato, Nat. Photonics **3**, 720 (2009); E. Nagali, D. Giovannini, L. Marrucci, E. Santamato, and F. Sciarrino, Phys. Rev. Lett. **105**, 073602 (2010).
[6] E. Karimi, B. Piccirillo, E. Nagali, L. Marrucci, and E. Santamato, Appl. Phys. Lett. **94**, 231124 (2009).
[7] E. Karimi, S. Slussarenko, B. Piccirillo, L. Marrucci, and E. Santamato, Phys. Rev. A **81**, 053813 (2010).
[8] P. G. de Gennes, *The Physics of Liquid Crystals* (Oxford University Press, Oxford, 1974); L. M. Blinov and V. G. Chigrinov, *Electrooptic Effects in Liquid Crystal Materials* (Springer, Berlin, 1996).
[9] An ac rather than a dc voltage is applied to avoid electrochemical degradation (Ref. 8).
[10] H. Hakemi, Mol. Cryst. Liq. Cryst. **287**, 215 (1996).
[11] H.-H. Liu and W. Lee, Appl. Phys. Lett. **97**, 023510 (2010).
[12] Z. Ran, P. Zeng-Hui, L. Yong-Gang, Z. Zhi-Gang, and X. Li, Chin. Phys. B **18**, 4380 (2009).

Tunable liquid crystal q-plates with arbitrary topological charge

Sergei Slussarenko,[1,*] Anatoli Murauski,[2] Tao Du,[2] Vladimir Chigrinov,[2] Lorenzo Marrucci,[1,3] and Enrico Santamato[1]

[1]*Dipartimento di Scienze Fisiche, Università di Napoli "Federico II", Complesso Universitario di Monte S. Angelo, 80126 Napoli, Italy*
[2]*Hong Kong University of Science and Technology, Clear Water Bay, Kowloon, Hong Kong*
[3]*CNR-SPIN, Complesso Universitario di Monte S. Angelo, I-80126 Napoli, Italy*
[*]*sergei.slussarenko@na.infn.it*

Abstract: Using a photoalignment technique with a sulphonic azo-dye as the surfactant aligning material, we fabricated electrically tunable liquid crystal q-plates with topological charge 0.5, 1.5 and 3 for generating optical vortex beams with definite orbital angular momentum (OAM) 1,3 and 6 per photon (in units of $\hbar$), respectively. We carried out several tests on our q-plates, including OAM tomography, finding excellent performances. These devices can have useful applications in general and quantum optics.

OCIS codes: (160.3710) Liquid crystals; (050.4865) Optical vortices.

References and links

1. L. Allen, M. W. Beijersbergen, R. J. C. Spreeuw, and J. P. Woerdman, "Orbital angular momentum of light and the transformation of Laguerre-Gaussian laser modes," Phys. Rev. A **45**, 8185–8189 (1992).
2. S. Franke-Arnold, L. Allen, and M. J. Padgett, "Advances in optical angular momentum," Laser Photon. Rev. **2**, 299–313 (2008).
3. A. Jesacher, S. Fürhapter, S. Bernet, and M. Ritsch-Marte, "Shadow effects in spiral phase contrast microscopy," Phys. Rev. Lett. **94**, 233902 (2005).
4. G. Gibson, J. Courtial, M. J. Padgett, M. Vasnetsov, V. Pasko, S. M. Barnett, and S. Franke-Arnold, "Free-space information transfer using light beams carrying orbital angular momentum," Opt. Express **12**, 5448–5456 (2004).
5. A. Mair, A. Vaziri, G. Welhs, and A. Zeilinger, "Entanglement of the angular momentum states of photons," Nature **412**, 313–315 (2001).
6. J. T. Barreiro, N. K. Langford, N. A. Peters, and P. G. Kwiat, "Generation of hyperentangled photon pairs," Phys. Rev. Lett. **95**, 260501 (2005).
7. G. Molina-Terriza, J. P. Torres, and L. Torner, "Twisted photons," Nat. Phys. **3**, 305–310 (2007).
8. L. Aolita and S. P. Walborn, "Quantum communication without alignment using multiple-qubit single-photon states," Phys. Rev. Lett. **98**, 100501 (2007).
9. M. W. Beijersbergen, R. P. C. Coerwinkel, M. Kristensen, and J. P. Woerdman, "Helical-wavefront laser beams produced with a spiral phaseplate," Opt. Commun. **112**, 321–327 (1994).
10. M. W. Beijersbergen, L. Allen, H. van der Veen, and J. P. Woerdman, "Astigmatic laser mode converters and transfer of orbital angular momentum," Opt. Commun. **96**, 123–132 (1993).
11. V. Y. Bazheov, M. S. Soskin, and M. V. Vasnetsov, "Screw dislocations in light wavefronts," J. Mod. Opt. **39**, 985–990 (1992).
12. Y. Igasaki, F. Li, N. Yoshida, H. Toyoda, T. Inoue, N. Mukohzaka, Y. Kobayashi, and T. Hara, "High efficiency electrically-addressable phase-only spatial light modulator," Opt. Rev. **6**, 339–344 (1999).
13. L. Marrucci, C. Manzo, and D. Paparo, "Optical spin-to-orbital angular momentum conversion in inhomogeneous anisotropic media," Phys. Rev. Lett. **96**, 163905 (2006).
14. L. Marrucci, C. Manzo, and D. Paparo, "Pancharatnam-Berry phase optical elements for wavefront shaping in the visible domain: switchable helical modes generation," Appl. Phys. Lett. **88**, 221102 (2006).
15. E. Karimi, B. Piccirillo, E. Nagali, L. Marrucci, and E. Santamato, "Efficient generation and sorting of orbital angular momentum eigenmodes of light by thermally tuned q-plates," Appl. Phys. Lett. **94**, 231124 (2009).

#136999 - $15.00 USD Received 22 Oct 2010; revised 10 Dec 2010; accepted 13 Dec 2010; published 16 Feb 2011

16. B. Piccirillo, V. DAmbrosio, S. Slussarenko, L. Marrucci, and E. Santamato, "Photon spin-to-orbital angular momentum conversion via an electrically tunable q-plate," Appl. Phys. Lett. arXiv:1010.4473 (in press).
17. E. Karimi, S. Slussarenko, B. Piccirillo, L. Marrucci, and E. Santamato, "Polarization-controlled evolution of light transverse modes and associated pancharatnam geometric phase in orbital angular momentum," Phys. Rev. A **81**, 053813 (2010).
18. E. Nagali, L. Sansoni, F. Sciarrino, F. De Martini, L. Marrucci, B. Piccirillo, E. Karimi, and E. Santamato, "Optimal quantum cloning of orbital angular momentum photon qubits through hong-ou-mandel coalescence," Nat. Photon. **3**, 720–723 (2009).
19. S. Nersisyan, N. Tabiryan, D. M. Steeves, and B. R. Kimball, "Fabrication of liquid crystal polymer axial waveplates for uv-ir wavelengths," Opt. Express **17**, 11926–11934 (2009).
20. P. G. de Gennes, *The Physics of Liquid Crystals* (Oxford University Press, Oxford, 1974).
21. The strong anchoring at both the sample walls prevents the decay of the otherwise unstable disclination lines with integer q.
22. V. G. Chigrinov, V. M. Kozenkov, and H.-S. Kwok, *Photoalignment of Liquid Crystalline Materials: Physics and Applications* (Wiley Publishing, 2008).
23. D. F. V. James, P. G. Kwiat, W. J. Munro, and A. G. White, "Measurement of qubits," Phys. Rev. A **64**, 052312 (2001).
24. The fidelity of the measured state $|\psi\rangle$ with respect to the expected state $|\psi_0\rangle$ is usually defined as $\langle\psi|\psi_0\rangle^2$.
25. B. Jack, J. Leach, H. Ritsch, S. M. Barnett, M. J. Padgett, and S. Franke-Arnold, "Precise quantum tomography of photon pairs with entangled orbital angular momentum," N. J. Phys. **11**, 103024 (2009).
26. E. Nagali, F. Sciarrino, F. De Martini, L. Marrucci, B. Piccirillo, E. Karimi, and E. Santamato, "Quantum information transfer from spin to orbital angular momentum of photons," Phys. Rev. Lett. **103**, 013601 (2009).

1. Introduction

A light beam has two "rotational" degrees of freedom: spin angular momentum (SAM) and orbital angular momentum (OAM). The first is associated to the polarization of the transverse electric field and may take the values $s = \pm\hbar$ per photon, that correspond to circular left and right polarization, respectively. OAM is associated to the phase structure of the complex electric field and paraxial beams with a helical phase front defined by the factor of $\exp(i\ell\varphi)$ carry a definite amount of OAM per photon equal to $\ell\hbar$, where ℓ can take any integer value [1,2]. In last years, beams carrying OAM have received an increased attention in classical [3,4] and quantum optics [5–8]. Till now, few methods of OAM-carrying beam generation were proposed, namely spiral phase plates [9], astigmatic lens converters [1,10] and computer generated fork holograms (CGH) [11] in conjunction with spatial light modulators (SLMs) [5,12]. All these methods have in terms of efficiency, working speed and stability or have specific requirements for the input light state.

Recently, a novel device based on liquid crystal (LC) technology, able to generate and manipulate the OAM was introduced [13,14]. This device, called "q-plate" (QP) is essentially a birefringent wave plate with inhomogeneous patterned distribution of the local optical axis in the transverse plane. The pattern of the optical axis distribution is defined by a semi-integer topological charge "q". When a circularly polarized light beam traverses the QP, a $\pm 2q$ amount of OAM (in units of $\hbar$) is transferred into the beam, with the sign determined by the input polarization helicity. The efficiency of this conversion is given by the optical retardation δ of the QP, that can be controlled by temperature [15] or electrical field, as made in this work [16]. QPs can be very efficient, fast and stable, although they are less flexible than SLMs as they address only a OAM two-dimensional subspace.

Till now, only $q = 1$ QPs were realized with LCs. Such device has already found a number of applications in various fields of optics [17,18]. Polymer based QPs were manufactured elsewhere [19], but such QPs, being solid and non-tunable, are suitable for single wavelength, require accurate control of thickness during manufacturing and cannot be used in applications where the conversion efficiency must be changed or switched. In this paper we report the realization of LC-based δ-tunable QPs with arbitrary topological charge by a photoalignment technology and demonstrate examples of QPs with $q = 0.5, 1.5$ and 3.

#136999 - $15.00 USD Received 22 Oct 2010; revised 10 Dec 2010; accepted 13 Dec 2010; published 16 Feb 2011

2. Q-plate structure and fabrication

In the QP, the LC film is enclosed between glass walls perpendicular to the z-axis. The orientation of the local optical axis of the QP is given by the LC molecular director distribution $\boldsymbol{n}(\boldsymbol{r}) = (\sin\theta\cos\alpha, \sin\theta\sin\alpha, \cos\theta)$, with $\theta = \theta(\boldsymbol{r}), \alpha = \alpha(\boldsymbol{r})$ being the polar angles. The walls of the QPs are coated for parallel strong anchoring ($\theta = \pi/2$) and the the surface alignment profile is made so to have $\alpha(x,y) = \alpha(\varphi) = q\varphi + \alpha_0$ in the LC bulk, where $\varphi = \arctan(y/x)$ is the transverse azimuthal coordinate, α_0 is a real number, and q is an integer or half integer number. The surface texture induced by this distribution is known in the physics of LC as a Schlieren structure with an isolated point defect (or "noyau") of topological charge q at the wall center [20]. The "noyaux" in the two walls of the cell are carefully aligned along the z axis during the cell manufacturing, so that a disclination line of same charge q is generated in the bulk (from here the name q-plate of the device). As it is well known from the elastic theory of LC, the equivalence between $\boldsymbol{n}$ and $-\boldsymbol{n}$ implies that the charge q is either integer or half-integer [21].

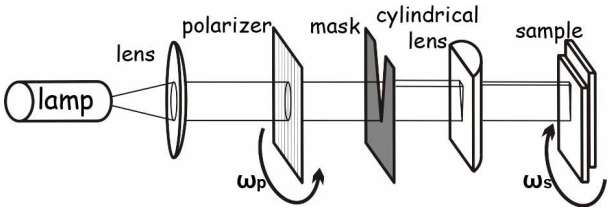

Fig. 1. (Color online) QP fabrication setup scheme.

The traditional way to manufacture a cell with planar alignment of liquid crystal is to rub the inner sides of the glass walls, previously coated with thin layer of polyimide, with velvet fabric. The rubbing direction defines the anisotropy of the surface that, in turn, orient the LC molecules perpendicular (or parallel, depending on the LC type) to the rubbing direction. The $q = 1$ QPs can be manufactured in this way, by rubbing the cell walls with a rotating piece of fabric [13, 15]. Other patterns, with $q \neq 1$ cannot be made by this method. In this work, we employed a photoalignment technique. The scheme of our setup is shown in Fig. 1. The LC cell was made from two glass substrates, spin-coated with 1% solution of sulphonic azo-dye SD1 (Dainippon Ink and Chemicals) in dimethylformamide (DMF) for 30 s at 3000 rpm. The glass windows were coated with conducting Indium-Tin-Oxide (ITO) to apply and external electrical field to the LC film. After the evaporation of the solvent, by soft-baking at 120 °C for 5 min, the glasses were assembled together and 6 m dielectric spacers were used to define the cell gap. A mercury lamp of 180 mW/cm^2 power density was used as the collimated light source. The light beam was polarized by a linear wiregrid polarizer and made to pass through an angular mask of 10° angular aperture. After the mask, a cylindrical lens was used to focus and converge the selected sector on the cell. The SD1 surfactant provides planar alignment for the LC in the direction perpendicular to the writing light polarization, with anchoring energy comparable with the polyimide rubbing based alignment [22]. Both polarizer and sample were attached to rotating mounts controlled by PC through step-motors. The rotation step of the sample was set to 2°. An exposure time of 2 hours and one complete turn of the sample was enough to provide high quality alignment of the LC film in all our QPs. Such values, together with the angular aperture of the mask, resulted from a compromise between having enough light passing through the mask and having a small enough image of the mask on the cell to obtain an acceptable smoothly varying local surface alignment. To make QPs with very large

#136999 - $15.00 USD Received 22 Oct 2010; revised 10 Dec 2010; accepted 13 Dec 2010; published 16 Feb 2011

q value smaller mask angular aperture would be necessary. By adjusting the ratio between the angular speeds of the two motors, different topological charges were impressed on the cell walls. It can be easily shown that the induced topological charge is given by $q = 1 \pm \frac{\omega_p}{\omega_s}$, where ω_p and ω_s are the angular speeds of the polarizer and sample, respectively, and the "+" and "−" signs correspond to opposite and same rotation direction of the two mounts, respectively. After the exposure, the samples were filled with the LC (MLC 6080 mixture from Merck) and sealed by epoxy glue. Heating the sample above the LC clearing point and subsequent slow cooling helped to remove occasional LC alignment defects. Topological charges $q = 0.5, 1.5, 3$, as shown in Fig. 2(a-c), were realized with the procedure described above. However any semi-integer charge can be realized, in principle, with this technique.

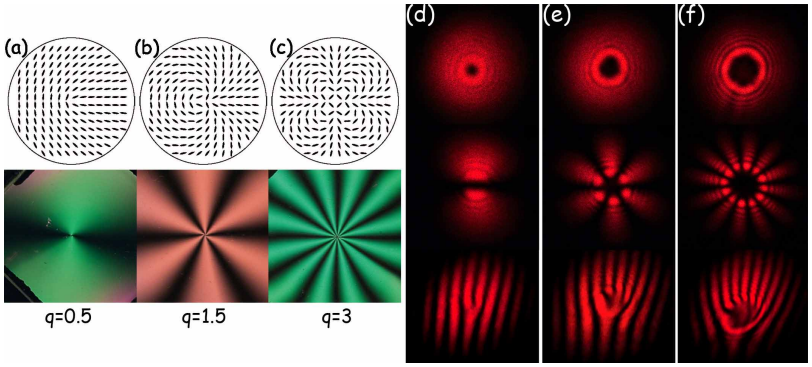

Fig. 2. (Color online) (a-c) Examples of the LC patterns with different topological charges and photos of the corresponding samples under crossed polarizers. (d-f) CCD pictures of the intensity beam profiles generated by the QPs shown in (a-c) when they are tuned. The input beam polarization was circularly polarized (top) or linearly polarized (middle). The respective interference patterns with a plane wave are also shown (bottom).

3. Optical characterization

When a beam traverses a QP with topological charge q and phase retardation δ, a fraction $\sin^2 \frac{\delta}{2}$ of the photons in the beam have their SAM reversed and change their OAM by an amount $\pm 2q$. More precisely, the photons flipping their spin from -1 to $+1$ (-1 to $+1$) change their OAM of $-2q$ ($+2q$). The remaining photon fraction $\cos^2 \frac{\delta}{2}$ remain in their initial SAM and OAM state. [13, 14] When the phase retardation of the QP is tuned to half-wave ($\delta = \pi$) all the input photons will be converted. In the particular case of charge $q = 1$, the total SAM+OAM light angular momentum remains unchanged in passing through the QP, so that the change of the photon SAM is transferred into a corresponding opposite change of the photon OAM, yielding a spin-to-OAM conversion (STOC) [13]. For a single photon, a similar action takes place on two wave-function components, with amplitudes $\sin \frac{\delta}{2}$ and $\cos \frac{\delta}{2}$ respectively.

The preliminary test on our QPs was just to observe the intensity pattern generated by the QP for a circularly or linearly polarized TEM_{00} incident beam. The observed intensity patterns are shown in Fig. 2(d-f, top and middle row). In the case of the circular polarization of the incident beam the we found the typical doughnut profile of vortex beam, while for the linear input polarization the intensity pattern shows a number $4q$ of bright radial lobes, as foreseen from theory. To better demonstrate the capability of our QPs to generate optical vortices a measurement of the helical phase front is desirable. Such measurement was done by inserting the QP into one arm of a Mach-Zehnder interferometer and by registering the interference pattern with a reference wave. The interference patterns, in the case of a plane reference wave

#136999 - $15.00 USD Received 22 Oct 2010; revised 10 Dec 2010; accepted 13 Dec 2010; published 16 Feb 2011

at small angle, have a typical "fork"-like structure [11], in which interference fringes have a disclination, where the optical vortex is located. The disclination order (i.e. the splitting of the interference line into a higher number of lines) corresponds to the OAM value of the beam, as shown in Fig. 2(d-f, bottom row). We tested also the STOC efficiency of our QPs, defined as the ratio between the STOC converted power and the total power in the output. This measurement was done by registering the power fraction of the light transmitted by the QP having polarization orthogonal to that of the incident beam. The QP conversion efficiency was changed by changing the QP retardation δ by applying an external voltage. To avoid electro-chemical effects, we applied a 2 kHz square-shaped voltage. The measurements were done at 543.5 nm and 633 nm light wavelengths. The results for the $q = 0.5$ QP are shown in Fig. 3(a). We obtained a STOC efficiency of up to 99% for all fabricated QPs. Due to unavoidable reflection, diffusion, and absorption losses in the QP, the overall STOC efficiency defined as the ratio between the STOC converted power in the output and the total incident power was found about 86% for all our QPs. These losses, however, could be easily avoided by adding an antireflection coating.

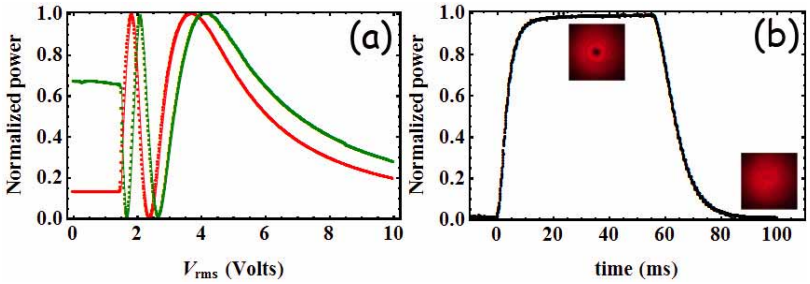

Fig. 3. (Color online) (a) – fraction of the output power converted by STOC in the QP as a function of the applied voltage. Red line - 633 nm input beam wavelength, green line - 534.5 nm input beam wavelength. (b) – time behavior of the QP upon sending two consecutive AC pulses that correspond to the minimum and maximum conversion efficiency. The intensity patterns in the insets show the on-off switching of the vortex beam with $\ell = 1$. The data refer to the QP with $q = 0.5$.

Since the STOC efficiency measurement was based on the polarization state of the beam only, an additional detailed study of the beam phase structure is required. For doing this we measured directly the OAM content of the beam generated by the QP, tuned to the maximum conversion, exploiting a tomographic technique [23]. Since we were not interested in the beam polarization, we fixed it by inserting a linear polarizer after the QP and carried out only the tomography of the beam OAM content. The main advantage of the optical tomography is that both amplitude and phase of the OAM components of a light beam can be reconstructed and that also the "fidelity" of the beam OAM state with respect to a given theoretical state can be evaluated [24]. Because the tomographic characterization is a very long procedure, we performed this test on the $q = 0.5$ QP only, restricting the OAM states to the Hilbert space spanned by the opposite OAM eigenvalues $\ell = \pm 1$. In the experiment, the $q = 0.5$ QP was used to generate the states $|1\rangle_o, |-1\rangle_o$, and $1/\sqrt{2}(|1\rangle_o - |-1\rangle_o)$, as described above, and a set of six computer-generated holograms (CGH) was sent into a spatial light modulator (SLM) to project the given beam state into the corresponding OAM bases [25,26]. The density matrices of the measured states are reported in Fig. 4(a)-(c). The measurements showed an average fidelity of $98 \pm 1\%$ of the generated states with the expected ones. We tested also the correlation between the circularly right polarized fraction of the beam coming from the $q = 0.5$ QP and the power of the $\ell = 1$ component of the same beam for different elliptically polarized states of the input TEM_{00} beam. The measurements were carried on with a circular polarizer to select the right handed

#136999 - $15.00 USD Received 22 Oct 2010; revised 10 Dec 2010; accepted 13 Dec 2010; published 16 Feb 2011

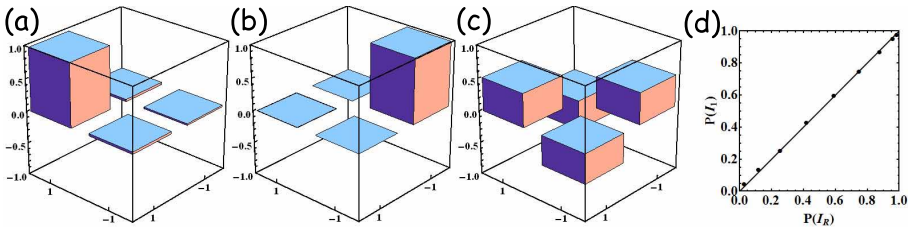

Fig. 4. (Color online) (a)-(c) – the real components of the density matrices of the OAM states, reconstructed via quantum tomography process for the $|1\rangle_o$, $|-1\rangle_o$ and $\frac{1}{\sqrt{2}}(|1\rangle_o - |-1\rangle_o)$ states respectively. (d) - fraction of the $\ell = 1$ beam intensity as the function of the fraction of the right polarized output beam, for different elliptically polarized inputs. The data refer to the QP with $q = 0.5$

polarization and a suitable fork hologram to select the $\ell = 1$ OAM component. The results are shown in Fig. 4(d). We found a standard deviation of $\sigma = 0.02$ from perfect one-to-one correlation between the circular right polarization state of photons and their OAM value $\ell = 1$. As the final test, we measured the switching speed of the QP with $q = 0.5$ between the last minimum conversion point where the output beam has $\ell = 0$ and the last maximum conversion point where the output beam has $\ell = 1$. These points are located at 2.4 and 3.7 Volts rms in Fig. 3, respectively (for 633 nm). The switching times were found to be around 25-30 ms, as shown in Fig. 3(b). The intensity profiles in the insets show the on-off switching of the vortex beam with $\ell = 1$.

4. Conclusions

In conclusion, using a photoalignment technique we realized several nematic liquid crystal QPs with the topological charge q different from $q = 1$, including fractionary half-integer charges. The optical phase retardation of our QPs can be tuned by external electric field, that allows to simplify the manufacturing procedure, removing particular requirements for the cell gap and reach high conversion efficiencies (up to 99%) for different wavelengths of the input light in real time. Our method is siutable for manufacturing tunable q-plates with arbitrary charge q.

Acknowledgments

Financial support from grants HKUST CERG 612208, CERG 612310, CERG 612409 and from the Seventh Framework Programme of the European Commission, under FET-Open grant number: 255914, "PHORBITECH", is gratefully acknowledged.

#136999 - $15.00 USD Received 22 Oct 2010; revised 10 Dec 2010; accepted 13 Dec 2010; published 16 Feb 2011

Laser-induced radial birefringence and spin-to-orbital optical angular momentum conversion in silver-doped glasses

Jafar Mostafavi Amjad,[1] Hamid Reza Khalesifard,[1] Sergei Slussarenko,[2] Ebrahim Karimi,[2,a)] Lorenzo Marrucci,[2,3] and Enrico Santamato[2]
[1]*Department of Physics, Institute for Advanced Studies in Basic Sciences (IASBS), 45137-66731 Zanjan, Iran*
[2]*Dipartimento di Scienze Fisiche, Università di Napoli "Federico II," Complesso Universitario di Monte S. Angelo, 80126 Napoli, Italy*
[3]*CNR-SPIN, Complesso di Monte S. Angelo, 80126 Napoli, Italy*

(Received 15 May 2011; accepted 23 June 2011; published online 8 July 2011)

Samples of Ag^+/Na^+ ion-exchanged glass that have been subject to intense laser irradiation may develop novel optical properties, as a consequence of the formation of patterns of silver nanoparticles and other structures. Here, we report the observation of a laser-induced permanent transverse birefringence, with the optical axis forming a radial pattern, as revealed by the spin-to-orbital angular momentum conversion occurring in a probe light beam. The birefringence pattern can be modeled well as resulting from thermally-induced stresses arising in the silver-doped glass during laser exposure, although the actual mechanism leading to the permanent anisotropy is probably more complex. © *2011 American Institute of Physics*. [doi:10.1063/1.3610474]

Metal-doped dielectrics may acquire interesting linear and nonlinear optical properties, arising from the combination of the dielectric transparency and of the metallic surface-plasmon-polariton (SPP) response, particularly when the metallic component aggregates in nanoparticles, clusters, or more complex structures, giving rise to a kind of self-assembled metamaterial.[1,2] The SPP resonances depend critically on the metal cluster size, shape, and distribution so that these materials can be effectively tailored to make novel functional devices for optoelectronics and telecommunications.[3–5] Silver-ion-exchanged glass is one of the most promising materials, due to its easy manufacturing and flexible properties. Different techniques have been demonstrated to control the silver cluster structure, size, distribution, and phase separation, most of which are based on applying a strong DC electric field or on exposing the materials to intense laser illumination.[2,6–10]

Recently, Nahal *et al*. reported that initially isotropic silver-doped glasses become birefringent under strong laser illumination during preparation, with the optical axis lying along the laser propagation direction.[11] In this paper, we report the observation that laser exposure generates also a significant transverse birefringence, with the induced optical axis forming a radial pattern around the laser beam axis. This pattern gives rise to optical depolarization effects occurring at small deflection angle (in contrast to the large-angle conoscopic effects reported in Ref. 11). We link these birefringence effects to a partial conversion of the spin angular momentum (SAM) of the incoming photons into orbital angular momentum (OAM), a process known as spin-to-orbital angular momentum conversion (STOC).[12,13] As a consequence of STOC, the SAM and OAM degrees of freedom of photons become entangled and the polarization becomes spatially variant, giving rise to the apparent depolarization of the light beam. It should be emphasized however that this form of depolarization is not originated by random dephasing, as in natural light sources, but it is a deterministic phenomenon that preserves the overall light coherence.

The investigated samples were prepared by the well known Ag^+/Na^+ ion exchange technique.[11,14,15] Soda-lime glass slides of dimensions $39 \times 25 \times 0.85$ mm merged into a 96:4 (weight ratio) molten mixture of $NaNO_3$ and $AgNO_3$ at 400 °C for 4 h. The chemical composition of the glass was: SiO_2, 80%; CaO, 9.41%; Na_2 O, 4.0%; MgO, 3.3%; Al_2O_3, 2.2%; K_2O, 0.41%; S, 0.2%; Fe_2O_3, 0.11%; P_2O_5, 0.11%; others, 0.26% (percentages in weight). The ion-exchanged glass samples were then irradiated with a multi-line Ar^+ laser beam focused onto a spot with a 3 mm diameter. Three samples were prepared with different exposure doses: 100 W/cm^2 for 1 s (S1), 30 W/cm^2 for 10 s (S2), and 100 W/cm^2 for 10 s (S3). These silver-doped glasses are moderately absorbing in the visible, so the laser beam leads to a strong local heating during exposure and to the development of a radial thermal gradient towards the center of the laser spot. This thermal gradient generates in turn a mechanical stress leading, by elasto-optic effect, to a cylindrically symmetric radial birefringence. In the case of a Gaussian beam profile, the birefringence pattern induced by this mechanism during exposure can be calculated analytically.[16,17] For an initially isotropic material such as glass, the local direction of the optical axis is radially oriented along the temperature gradient and the local optical birefringent retardation δ is radially symmetric and given by

$$\delta(r) = \delta_0 \left[1 + \frac{1}{2} \left(\frac{r_0}{r} \right)^2 \left(e^{-\frac{2r^2}{r_0^2}} - 1 \right) \right], \qquad (1)$$

where r is the radial coordinate, r_0 is the waist radius of the laser beam, and δ_0 is the asymptotic phase retardation for large radii. The latter will depend on the glass thermal, optical, and elasto-optical properties and on the light power. In our case, the actual mechanism leading to the radial birefringence must clearly be more complicated than that described

a)Electronic mail: karimi@na.infn.it.

above, because during laser irradiation, the Ag^+ ions are known to form nano-clusters which migrate around the beam axis, contributing to the induced optical anisotropy. In addition, the laser-induced thermal stresses can deform the surface of the glass sample, producing a lensing effect. Once the laser light is turned off and the sample cools down, the silver-particle distribution, stresses, and surface deformation are frozen, and the radial birefringence thus becomes persistent. A detailed model of these rather complex effects is under investigation, but it is reasonable to assume that Eq. (1) remains approximately valid as a phenomenological model, with parameters δ_0 and r_0 now depending also on the laser intensity and exposure time and on the Ag^+ ion concentration and mobility.

The main optical effect of the birefringence pattern given by Eq. (1) can be simply obtained using the Jones operator, $\hat{U}$, acting on the light polarization. In the basis of the circular polarizations, the Jones operator $\hat{U}$ assumes the simple form

$$\hat{\mathrm{U}} \cdot |\pm\rangle = \cos\left[\frac{\delta(r)}{2}\right]|\pm\rangle - i\sin\left[\frac{\delta(r)}{2}\right]|\mp\rangle e^{\pm 2i\phi}, \quad (2)$$

where $|+\rangle$ and $|-\rangle$ denote the left and right circular polarizations, respectively, and ϕ is the azimuthal angle in the transverse plane. As we see, if the input light is circularly polarized, the transmitted light will be the superposition of an unmodified wave, with amplitude reduced by the factor $\cos(\delta/2)$, and a new wave having opposite polarization handedness, with amplitude factor $\sin(\delta/2)$. The latter also exhibits a vortex phase factor $e^{\pm 2i\phi}$, corresponding to an OAM of $\pm 2\hbar$ per photon, exactly balancing the variation of SAM (i.e., from $\pm\hbar$ to $\mp\hbar$): this is just the STOC process.[12,13] In the following, for brevity, the polarization-inverted component with nonzero OAM (assuming that the input has zero OAM) will be referred to as the "STOC component" of the outgoing light.

The polarization of the STOC component is always orthogonal to the polarization of the input beam, which explains the observed depolarization of the transmitted light. Depolarization occurs for any input polarization (linear or elliptical), since any polarization can be decomposed into the left and right circular components, each undergoing STOC to a different (opposite) OAM value, so after STOC they do not add up coherently anymore. The STOC efficiency is given by $\sin^2[\delta(r)/2]$. Therefore, complete STOC is expected only for certain radii, determined by the Eq. $\delta(r) = (2n + 1)\pi$ with n integer, with partial STOC elsewhere. Because in the present case, $\delta(r)$ is not small generally, this varying STOC efficiency should give rise to a radially-oscillating intensity profile of the transmitted STOC beam.

The optical properties acquired by our samples after the laser-induced effects described above have become permanent were studied using a probe laser beam having a Gaussian input profile with a beam waist diameter of about 4 mm, for two different input polarizations: left-circular and linear. In both cases, in transmission, we observed a large far-field ring pattern, which is typical of transverse phase-modulation, as observed also by other authors and due to the isotropic laser-induced modulation of optical properties.[10] The depolarized light, however, appears only in a small circular region around the pattern center that we selected by using an iris and a crossed polarizer. Figures 1(b) and 1(e) show the experimental intensity patterns of this depolarized light, for two different input polarizations. These patterns are very well reproduced by our calculations of the STOC component based on our model, as shown in Figs. 1(a) and 1(d). In the case of input circular polarization, in particular, the intensity profile is cylindrically symmetric and presents a dark singularity at the center, characteristic of a beam carrying nonzero OAM. Moreover, the patterns exhibit concentric circular fringes resulting from the radial modulation of STOC efficiency, as discussed above. We also recorded the interference patterns resulting from the superposition of the depolarized light from the samples with a reference Gaussian beam (having the same polarization), in order to check the optical phase distribution. The interference pattern obtained for a circular polarization, in particular, presented the characteristic double spiral pattern, confirming that the OAM eigenvalue is $|\ell| = 2$, in units of $\hbar$.[12]

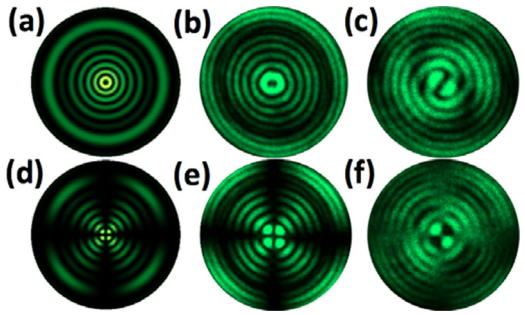

FIG. 1. (Color online) Far-field intensity profiles of a Gaussian probe light beam passing through sample S3. Upper panels are for a left-circular input polarization, lower panels for linear polarization (vertical in the figures). Panels (a) and (d) are the profiles calculated from our theory, (b) and (e) are the experimental ones, and (c) and (f) are interference patterns with a Gaussian reference beam. In the calculated patterns, we set $\delta_0 = 45$ and $r_0 = 0.7$ mm and assumed a probe beam waist of 2 mm.

We investigated the behavior of the overall STOC efficiency (defined as the power ratio between the space-integrated STOC component and the overall transmitted light) for our different samples, having different exposure parameters. Figure 2 shows that the overall STOC efficiency is an increasing function of the light energy dose absorbed by the

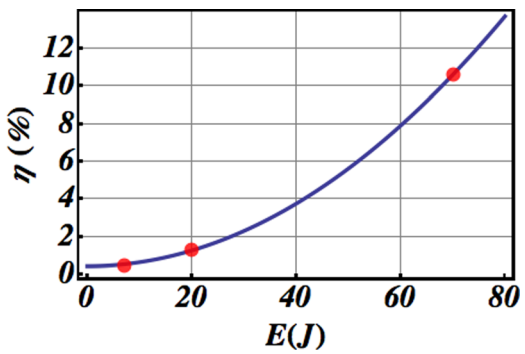

FIG. 2. (Color online) The STOC efficiency as a function of the total light energy deposited during the sample preparation. The circles correspond to the measured efficiency in our three samples S1, S2, and S3. The curve is a best fit with the quadratic expression $\eta(E) = a + bE^2$.

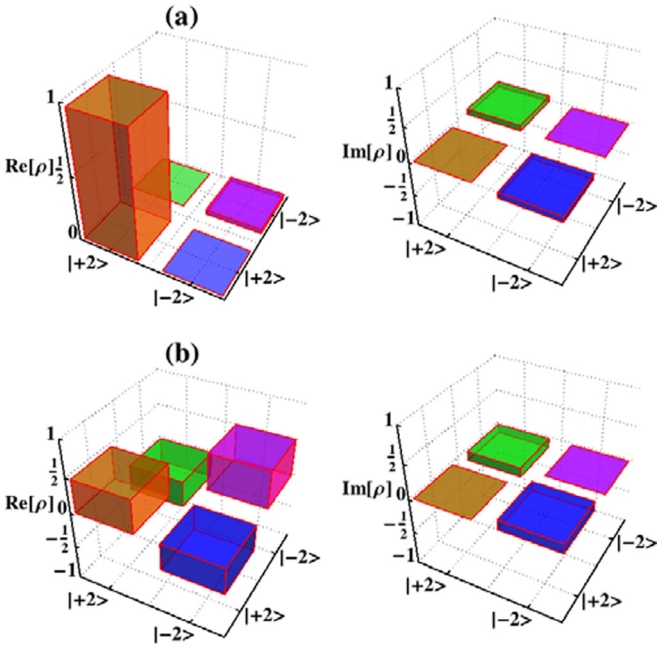

FIG. 3. (Color online) Experimental density matrix for a (a) left-circularly polarized and (b) linearly polarized input probe beam, as emerging from sample S3. Left and right panels show the real and imaginary part of the density matrix, respectively (but, within the experimental errors, all measured density-matrix elements were found to be real).

sample during its preparation, as could be reasonably expected.

The images shown in Fig. 1 provide a first qualitative confirmation of the occurrence of STOC in our samples. A more quantitative analysis can be performed by applying the methods of quantum tomography to reconstruct the probe photon OAM quantum state at the exit of the sample. This method allows us to retrieve both the amplitudes and relative phases of all OAM components of the transmitted light beam, despite the fact that they do not interfere. Our model predicts that, for any input polarization, only superpositions of OAM eigenstates with $\ell = \pm 2$ should be generated. Therefore, only the two-dimensional OAM Hilbert subspace spanned by $\ell = \pm 2$ is relevant. This space is isomorphous to the polarization space, so we may use "Stokes-like" parameters to describe it. The correspondence between the OAM and polarization spaces can be made by associating the OAM eigenstates $\ell = \pm 2$ with the left and right polarization states, respectively, and any superposition of the OAM eigenstates $\ell = \pm 2$ with the corresponding elliptical polarization state. Thus, just as in the case of polarization, to gain full information on the OAM state, we need only four independent measurements of the Stokes' parameters S_i $(i = 0,\ldots, 3)$, from which the full density matrix of the state can be retrieved.[18] To measure all OAM Stokes-like parameters, we used six gray-scale computer-generated holograms (CGH), as reported elsewhere.[19] These holograms were displayed in turn on a spatial light modulator (SLM) on which the depolarized light from the sample was made to impinge. The resulting far-field intensity in the central area of the first-order diffraction was then measured for each CGH and, by combining these data, all Stokes-like parameters were calculated.[19] The results of this OAM photon state tomography for the two cases of left-circular and linear input polarization of the probe beam are shown in Fig. 3, which presents the real and imaginary parts of the OAM density matrix. As we see, in the case of the left circular input polarization, all output photons of the depolarized component were put into the $\ell = +2$ OAM eigenstate (confirming again the STOC effect), while in the case of the vertical input polarization, we obtained an equal-weight coherent superposition of the two $\ell = \pm 2$ OAM eigenstates. Moreover, the fidelities of these states with the optical-field azimuthal profiles of ideal $|\ell| = 2$ and $(|\ell = 2\rangle + |\ell = -2\rangle)/\sqrt{2}$ modes were found to be 0.97 and 0.91, respectively. This confirms that the experimental results are in excellent agreement with our STOC-based model.

In conclusion, we have reported the appearance of a radial birefringence pattern in laser-exposed ion-exchanged silver-doped glasses, as demonstrated by the occurrence of spin-to-orbital angular momentum conversion in a probe beam. This pattern presumably arises as a result of laser-induced thermal gradients and ensuing silver nano-particle migration and permanently induced mechanical stresses in the glass.

We acknowledge the financial support of the FET-Open program within the 7*th* Framework Programme of the European Commission under Grant No. 255914, Phorbitech, and of IASBS research council under the Grant No. G2002IASBS101.

[1]U. Kreibig and M. Vollmer, *Optical Properties of Metal Clusters*, Springer series in Materials Science Vol. **25** (Springer, Berlin, 1995).
[2]A. Abdolvand, A. Podlipensky, S. Matthias, F. Syrowatka, U. Gösele, G. Seifert, and H. Graener, Adv. Mater. **17**, 2983 (2005).
[3]J. Auxier, S. Honkanen, A. Schülzgen, M. Morrell, M. Leigh, S. Sen, N. Borrelli, and N. Peyghambarian, J. Opt. Soc. Am. B **23**, 1037 (2006).
[4]F. Gonella, G. Mattei, P. Mazzoldi, E. Cattaruzza, G. W. Arnold, G. Battaglin, P. Calvelli, R. Polloni, R. Bertoncello, and R. F. Haglund, Appl. Phys. Lett. **69**, 3101 (1996).
[5]S. Friberg and P. Smith, IEEE J. Quantum Electron. **23**, 2089 (1987).
[6]F. Stietz, Appl. Phys. A: Mater. Sci. Process. **72**, 381 (2001).
[7]R Jin, Y. Cao, E. Hao, G. S. Métraux, G. C. Schatz, and C. A. Mirkin, Nature **425**, 487 (2003).
[8]A. Nahal, J. Mostafavi-Amjad, A. Ghods, M. R. H. Khajehpour, S. N. S. Reihani, and M. R. Kolahchi, J. Appl. Phys. **100**, 1063 (2006).
[9]A. Miotello, Appl. Phys. Lett. **79**, 2456 (2001).
[10]Y. Kaganovskii, I. Antonov, F. Bass, M. Rosenbluh, and A. Lipovskii, J. Appl. Phys. **89**, 8273 (2001).
[11]A. Nahal and F. Moslehirad, J. Mater. Sci. **42**, 9075 (2007).
[12]L. Marrucci, C. Manzo, and D. Paparo, Phys. Rev. Lett. **96**, 163905 (2006).
[13]L. Marrucci, E. Karimi, S. Slussarenko, B. Piccirillo, E. Santamato, E. Nagali, and F. Sciarrino, J. Opt. **13**, 064001 (2011).
[14]A. Nahal and H. R. Khalesifard, Opt. Mater. **29**, 987 (2007).
[15]S. I. Najafi, *Introduction to Glass Integrated Optics*, edited by S. I. Najafi (Artech House Publishers, 1992).
[16]E. Khazanov, O. V. Kulagin, S. Yoshida, D. B. Tanner, and D. H. Reitze, IEEE J. Quantum Electron. **35**, 1116 (1999).
[17]S. Mosca, B. Canuel, E. Karimi, B. Piccirillo, L. Marrucci, R. De Rosa, E. Genin, L. Milano, and E. Santamato, Phys. Rev. A **82**, 043806 (2010).
[18]M. Padgett and J. Courtial, Opt. Lett. **24**, 430 (1999).
[19]E. Nagali, F. Sciarrino, F. De Martini, B. Piccirillo, E. Karimi, L. Marrucci, and E. Santamato, Opt. Express **17**, 18745 (2009).

Polarization pattern of vector vortex beams generated by *q*-plates with different topological charges

Filippo Cardano,[1] Ebrahim Karimi,[1,*] Sergei Slussarenko,[1] Lorenzo Marrucci,[1,2] Corrado de Lisio,[1,2] and Enrico Santamato[1,3]

[1]Dipartimento di Scienze Fisiche, Università di Napoli "Federico II", Complesso di Monte S. Angelo, 80126 Napoli, Italy

[2]CNR-SPIN, Complesso Universitario di Monte S. Angelo, 80126 Napoli, Italy

[3]CNISM-Consorzio Nazionale Interuniversitario per le Scienze Fisiche della Materia, Napoli, Italy

*Corresponding author: karimi@na.infn.it

Received 5 December 2011; accepted 23 December 2011;
posted 3 January 2012 (Doc. ID 159438); published 5 March 2012

We describe the polarization topology of the vector beams emerging from a patterned birefringent liquid crystal plate with a topological charge q at its center (q-plate). The polarization topological structures for different q-plates and different input polarization states have been studied experimentally by measuring the Stokes parameters point-by-point in the beam transverse plane. Furthermore, we used a tuned $q = 1/2$-plate to generate cylindrical vector beams with radial or azimuthal polarizations, with the possibility of switching dynamically between these two cases by simply changing the linear polarization of the input beam.

OCIS codes: 050.4865, 260.6042, 260.5430, 160.3710.

1. Introduction

The polarization of light is a consequence of the vectorial nature of the electromagnetic field and is an important property in almost every photonic application, such as imaging, spectroscopy, nonlinear optics, near-field optics, microscopy, particle trapping, micromechanics, etc. Most past research dealt with scalar optical fields, where the polarization was taken uniform in the beam transverse plane. More recently, the so-called vector beams were introduced, where the light polarization in the beam transverse plane is space-variant [1]. As compared with homogeneously polarized beams, vector beams have unique features. Of particular interest are the singular vector beams where the polarization distribution in the beam transverse plane has a vectorial singularity as a *C*-point or *L*-line, where the azimuth angle and orientation of polarization ellipses are undefined, respectively [2,3]. The polarization singular points are often coincident with corresponding singular points in the optical phase, thus creating what are called vector vortex beams. Vector vortex beams are strongly correlated to singular optics, where the optical phase at a zero point of intensity is undetermined [4], and to light beams carrying definite orbital angular momentum (OAM) [5]. Among vector vortex beams, radially or azimuthally polarized vector beams have received particular attention for their unique behavior under focusing [6–8] and have been proved to be useful for many applications such as particle acceleration [9], single molecule imaging [10], nonlinear optics [11], coherent anti-Stokes Raman scattering microscopy [12], and particle trapping and manipulation [13]. Because of their cylindrical symmetry, the vector beams with radial and azimuthal polarization are also named cylindrical vector beams [1].

The methods to produce vector beams can be divided into active and passive. Active methods are based on the output of novel laser sources with specially designed optical resonators [14–16]. The

1559-128X/12/1000C1-06$15.00/0

passive methods use either interferometric schemes [17] or mode-forming holographic and birefringent elements [6,18–22]. Light polarization is usually thought to be independent of other degrees of freedom of light, but it has been shown recently that photon spin angular momentum (SAM) due to the polarization can interact with the photon OAM when the light propagates in a homogenous [23] and an inhomogenous birefringent plate [24,25]. Such interaction, indeed, gives the possibility to convert the photon spin into OAM and *vice versa* in both classical and quantum regimes [26].

In this work, to create optical vector beams we exploit the spin-to-OAM coupling in a birefringent liquid crystal plate with a topological charge q at its center, named "q-plate" [24,25]. As will be shown later, there are a number of advantages in using q-plates, mainly because the polarization pattern impressed in the output beam can be easily changed by changing the polarization of the incident light [27,28], and q-plates can be easily tuned to optimal conversion by external temperature [29] or electric fields [30,31]. Subsequently, the structure and quality of the produced vector field have been analyzed by point-by-point Stokes parameters tomography in the beam transverse plane for different q-plates and input polarization states. In particular, we generated and studied in detail the radial and azimuthal polarizations produced by a q-plate with fractional topological charge $q = 1/2$.

2. Polarization Topology

Henry Poincaré presented a nice pictorial way to describe the light polarization based on the $2 \to 1$ homomorphism of SU(2) and SO(3). In this description, any polarization state is represented by a point on the surface of a unit sphere, named a "*Poincaré*" or "*Bloch*" sphere. The light polarization state is defined by two independent real variables (ϑ, φ), ranging in the intervals $[0, \pi]$ and $[0, 2\pi]$, respectively, which fix the colatitude and azimuth angles over the sphere. An alternative algebraic representation of the light polarization state in terms of the angles (ϑ, φ) is given by

$$|\vartheta, \varphi\rangle = \cos\left(\frac{\vartheta}{2}\right)|L\rangle + e^{i\varphi}\sin\left(\frac{\vartheta}{2}\right)|R\rangle, \tag{1}$$

where $|L\rangle$ and $|R\rangle$ stand for the left- and right-circular polarizations, respectively. On the Poincaré sphere, north and south poles correspond to left- and right-circular polarization, respectively, while any linear polarization lies on the equator, as shown in Fig. 1(a). Special linear polarization states are the $|H\rangle$, $|V\rangle$, $|D\rangle$, and $|A\rangle$, which denote horizontal, vertical, diagonal, and antidiagonal polarizations, respectively. In points different from the poles and the equator, the polarization is elliptical with left (right)-handed ellipticity in the north (south) hemisphere.

An alternative mathematical description of the light polarization state, which is based on SU(2) representation, was given by George Gabriel Stokes in 1852. In this representation, four parameters S_i $(i = 0, \ldots, 3)$, now known as Stokes parameters, are exploited to describe the polarization state. This representation is useful, since the parameters S_i are simply related to the light intensities $I_p (p = L, R, H, V, D, A)$ measured for different polarizations, according to

$$\begin{aligned} S_0 &= I_L + I_R, \\ S_1 &= I_H - I_V, \\ S_2 &= I_A - I_D, \\ S_3 &= I_L - I_R. \end{aligned} \tag{2}$$

The Stokes parameters can be used to describe partial polarization too. In the case of fully polarized light, the reduced Stokes parameters $s_i = S_i/S_0 (i = 1, 2, 3)$ can be used instead. We may consider the reduced parameters s_i as the Cartesian coordinates on the Poincaré sphere. The s_i are normalized to $\sum_{i=1}^{3} s_i^2 = 1$. The states of linear polarization, lying on the equator of the Poincaré sphere, have $s_3 = 0$.

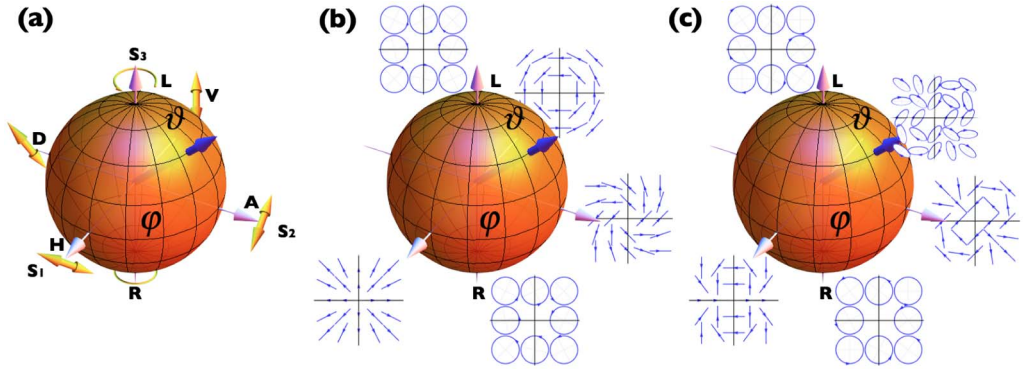

Fig. 1. (Color online) (a) Poincaré sphere representation for the polarization of a light beam with uniform transverse phase distribution. North (south) pole and equator correspond to left (right)-circular and linear polarizations, respectively. The other points have elliptical polarization, and antipodal points are orthogonal to each other. (b) and (c) show the polarization distribution in the transverse plane for $m = 1$ and $m = 2$, respectively, on the higher-order Poincaré sphere introduced in [32,33].

The two states $s_3 = \pm 1$ correspond to the poles and are circularly polarized. In singular optics, these two cases may form two different types of polarization singularities. For the other states, the sign of s_3 fixes the polarization helicity—left-handed for $s_3 > 0$ and right-handed for $s_3 < 0$. The practical advantages of using the parameters s_i are that they are dimensionless and depend on the ratio among intensities. Light intensities can be easily measured by several photodetectors and can be replaced by average photon counts in the quantum optics experiments. Thus, Stokes analysis provides a very useful way to perform the full tomography of the polarization state (Eq. (1)) in both classical and quantum regimes.

The passage of light through optical elements may change its polarization state. If the optical element is fully transparent, the incident power is conserved, and only the light polarization state is affected. The action of the transparent optical element is then described by a unitary transformation on the polarization state $|\vartheta, \varphi\rangle$ in Eq. (1) and corresponds to a continuous path on the Poincaré sphere. In most cases, the optical element can be considered so thin that the polarization state is seen to change abruptly from one point P_1 to a different point P_2 on the sphere. In this case, it can be shown that the path on the sphere is the geodetic connecting P_1 to P_2 [34]. Examples of devices producing a sudden change of the light polarization in passing through are half-wave (HW) and quarter-wave (QW) plates. A sequence of HW and QW can be used to move the polarization state on the whole Poincaré sphere, which corresponds to arbitrary SU(2) transformation applied to the $|\vartheta, \varphi\rangle$ state in Eq. (1). A useful sequence QW-HW-QW-HW (QHQH) to perform arbitrary SU (2) transformation on the light polarization state is presented in [28].

So far, we have considered an optical phase that is uniform in the beam transverse plane. Allowing for a nonuniform distribution of the optical phase between different electric field components gives rise to polarization patterns, such as azimuthal and radial ones, where special topologies appear in the transverse plane. The topological structure of the polarization distribution, moreover, remains unchanged while the beam propagates. It is worth noting that most singular polarization patterns in the transverse plane can still be described by polar angles ϑ, φ on the Poincaré sphere [32,33]. The points on the surface of this higher-order Poincaré sphere represent polarized light states where the optical field changes as $e^{\pm im\phi}$, where m is a positive integer and $\phi = \arctan(y/x)$ is the azimuthal angle in the beam transverse plane. As is well known, light beams with optical field proportional to $e^{im\phi}$ are vortex beams with topological charge m, which carry a definite OAM $\pm m\hbar$ per photon along their propagation axis. Because the beam is polarized, it carries SAM too, so that the photons are in what may be called a spin-orbit state. Among the spin-orbit states, only a few states can be described by the higher-order Poincaré sphere and, precisely, the states belonging to the spin-orbit SU (2)-subspace spanned by the two base vectors $\{|L\rangle e^{im\phi}, |R\rangle e^{-im\phi}\}$. In this representation, the north pole, south pole, and equator correspond to the base state $\{|L\rangle e^{im\phi}\}$, the base state $\{|R\rangle e^{-im\phi}\}$, and the linear polarization with rotated topological structure of charge m, respectively. Figures 1(b) and 1(c) show the polarization distribution for $m = 1$ and $m = 2$ spin-orbit subspaces, respectively. The intensity profile for all points on the higher-order Poincaré sphere has the same doughnut shape. The states along the equator are linearly polarized doughnut beams with topological charge m, differing in their orientation only.

3. The *q*-Plate: Patterned Liquid crystal Cell for Generating and Manipulating Helical Beam

The q-plate is a liquid crystal cell patterned in specific transverse topology, bearing a well-defined integer or semi-integer topological charge at its center [24,25,27]. The cell glass windows are treated so as to maintain the liquid crystal molecular director parallel to the walls (planar strong anchoring) with nonuniform orientation angle $\alpha = \alpha(\rho, \phi)$ in the cell transverse plane, where ρ and ϕ are the polar coordinates. Our q-plates have a singular orientation with topological charge q, so that $\alpha(\rho, \phi)$ is given by

$$\alpha(\rho, \phi) = \alpha(\phi) = q\phi + \alpha_0, \tag{3}$$

with integer or semi-integer q and real α_0. This pattern was obtained with an azo-dye photo-alignment technique [31]. Besides its topological charge q, the behavior of the q-plate depends on its optical birefringent retardation δ. Unlike other LC based optical cells [22] used to produce vector vortex beam, the retardation δ of our q-plates can be controlled by temperature control or electric field [29,30]. A simple argument based on the Jones matrix shows that the unitary action $\hat{U}$ of the q-plate in the state (1) is defined by

$$\hat{U}\begin{pmatrix} |L\rangle \\ |R\rangle \end{pmatrix} = \cos\frac{\delta}{2}\begin{pmatrix} |L\rangle \\ |R\rangle \end{pmatrix} + \mathrm{i}\,\sin\frac{\delta}{2}\begin{pmatrix} |R\rangle e^{+2i(q\phi+\alpha_0)} \\ |L\rangle e^{-2i(q\phi+\alpha_0)} \end{pmatrix}. \tag{4}$$

The q-plate is said to be tuned when its optical retardation is $\delta = \pi$. In this case, the first term of Eq. (4) vanishes, and the optical field gains a helical wavefront with double of the plate topological charge ($2q$). Moreover, the handedness of helical wavefront depends on the helicity of input circular polarization, positive for left-circular and negative for right-circular polarization.

4. Experiment

In our experiment, a TEM_{00} HeNe laser beam ($\lambda = 632.8$ nm, 10 mW) was spatially cleaned by focusing into a 50 μm pinhole followed by a truncated lens and polarizer in order to have a uniform intensity and a homogeneous linear polarization; see

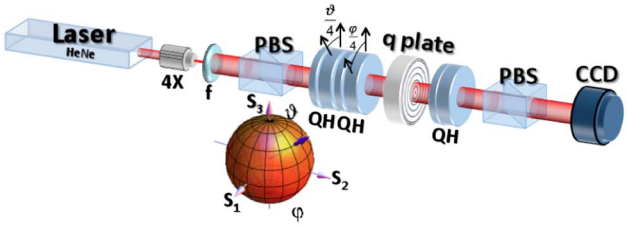

Fig. 2. (Color online) Setup to generate and analyze different polarization topologies generated by a q-plate. The polarization state of the input laser beam was prepared by rotating the two HW plates in the QHQH set at angles $\vartheta/4$ and $\varphi/4$ to produce a corresponding rotation of (ϑ, φ) on the Poincaré sphere, as indicated in the inset. The waveplates and polarizer beyond the q-plate were used to project the beam polarization on the base states (R, L, H, V, A, D) shown in Fig. 1(a). For each state projection, the intensity pattern was recorded by CCD camera, and the signals were analyzed pixel-by-pixel to reconstruct the polarization pattern in the beam transverse plane. Legend: 4×, microscope objective of 4× used to clean the laser mode; f, lens; Q, quarter-wave plate; H, half-wave plate; PBS, polarizing beam-splitter.

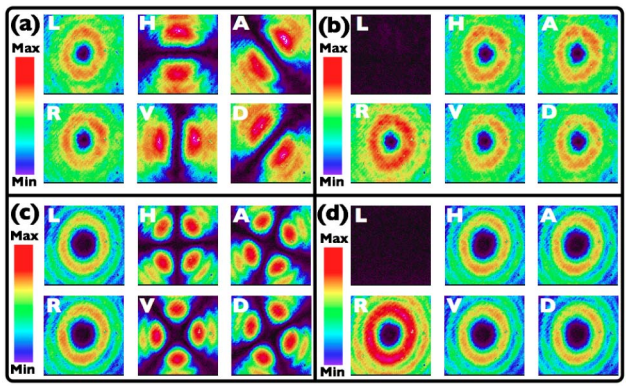

Fig. 3. (Color online) Recorded intensity profiles of the beam emerging from the q-plate projected over horizontal (H), vertical (V), antidiagonal (A), diagonal (D), left-circular (L), and right-circular (R) polarization base states for different q-plates and input polarizations. (a) and (b) are for the $q = 1/2$-plate, and horizontal-linear (a) and left-circular (b) polarization of the input beam. (c) and (d) are the same for the $q = 1$-plate. The color scale bar shows the intensity scale (arbitrary units) in false colors.

Fig. 2. The beam polarization was then manipulated by a sequence of wave plates as in [28] to reach any point on the Poincaré sphere. The beam was then sent into an electrically driven q-plate, which changed the beam state into an entangled spin-orbit state as given by Eq. (4). When the voltage on the q-plate was set for the optical tuning, the transmitted beam acquired the characteristic doughnut shape with a hole at its center. The output beam was analyzed by point-to-point polarization tomography, by projecting its polarization into the H, V, A, D, L, R sequence of basis and measuring the corresponding intensity at each pixel of a 120 × 120 resolution CCD camera (Sony AS-638CL). Examples of the recorded intensity profiles are shown in Fig. 3. A dedicated software was used to reconstruct the polarization distribution on the beam transverse plane. To minimize the error due to a small misalignment of the beam when the polarization was changed, the values of the measured Stokes parameters were averaged over a grid of 20 × 20 squares equally distributed over the image area. No other elaboration of the raw data nor the best fit with theory was necessary.

We analyzed the beams generated by two different q-plates with charges $q = 1/2$ and $q = 1$ for two different input polarization states. The q-plate optical retardation was optimally tuned for $\lambda = 632.8$ nm by applying an external voltage of a few volts [31]. We considered left-circular ($|L\rangle$) and linear-horizontal ($|H\rangle$) polarized input beams. These states, after passing through the q-plate, are changed into $|R, +2q\rangle$ and $(|R, +2q\rangle + |L, -2q\rangle)/\sqrt{2}$, respectively. Figure 3 shows the output intensity patterns for different

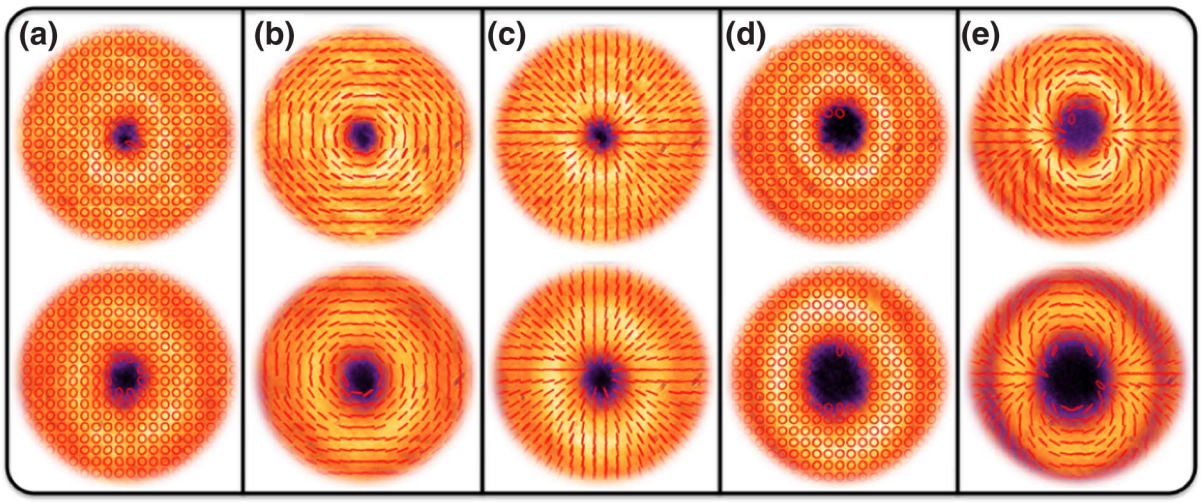

Fig. 4. (Color online) Highest-row panels: the transverse polarization and intensity distribution in the near field at the exit face of the q-plate. Lower panels: the polarization and intensity distributions in the far field beyond the q-plate. (a), (b), and (c) Polarization topological structure generated by the $q = 1/2$-plate for left-circular, V-linear, and H-linear input polarizations, respectively. (d) and (e) Polarization topological structure generated by the $q = 1$-plate for left-circular and H-linear input polarizations, respectively. (a) and (d) have uniform circular polarization distributions.

polarization selections. Figures 3(a) and 3(b) show the results of point-by-point polarization tomography of the output from $q = 1/2$-plate for left-circular and horizontal-linear input polarizations, respectively. Figures 3(c) and 3(d) show the results of point-by-point polarization tomography of the output from $q = 1$-plate for left-circular and horizontal-linear polarizations, respectively.

The case of $q = 1/2$-plate is particularly interesting, because for a linear-horizontal input polarization, it yields to the spin-orbit state $(|R, +1\rangle + |L, -1\rangle)/\sqrt{2}$ represented by the S_1-axes over the equator of the higher-order Poincaré sphere (Fig. 1(b)), which corresponds to a radially polarized beam, as shown in Fig. 4(c). This radial polarization can be changed into the azimuthal polarization (corresponding to the antipodal point on S_1-axes of the higher-order Poincaré sphere) by just switching the input linear polarization from horizontal to vertical, as shown in Fig. 4(b). This provides a very fast and easy way to switch from radial to azimuthal cylindrical vector beam. As previously said, cylindrical vector beams have a number of applications and can be used to generate uncommon beams such as electric and magnetic needle beams, where the optical field is confined below diffraction limits. Such beams have a wide range of applications in optical lithography, data storage, material processing, and optical tweezers [6,7].

Before concluding, it is worthwhile to mention that vortex vector beams are based on nonseparable optical modes, which is itself an interesting concept in the framework of classical optics. At the single photon level, however, the same concept has even more fundamental implications, because it is at the basis of the so-called quantum contextuality [35].

5. Conclusion

We have generated and analyzed a few vector vortex beams created by a patterned liquid crystal cell with topological charge, named q-plate. Radial and azimuthal cylindrical beams have been obtained by acting on the polarization of a traditional laser beam sent through a $q = 1/2$-plate. In this way, fast switching from the radial to the azimuthal polarization can be easily obtained. Finally, we studied in detail the polarization of a few vector beams generated by different q-plates, and the polarization distribution patterns have been reconstructed by point-by-point Stokes tomography over the entire transverse plane.

In this paper, however, we have investigated the cases $q = 1$ and $q = 1/2$. Future work will address other cases, and in particular the negative q ones.

We acknowledge the financial support of the FET-Open program within the 7th Framework Programme of the European Commission under grant 255914, Phorbitech.

References

1. Q. Zhan, "Cylindrical vector beams: from mathematical concepts to applications," Adv. Opt. Photon. **1**, 1–57 (2009).
2. J. F. Nye, *Natural Focusing and the Fine Structure of Light* (IOP Publishing, 1999).
3. M. R. Dennis, K. O'Holleran, and M. J. Padgett, "Optical vortices and polarization singularities," Prog. Opt. **53**, 293–363 (2009).
4. M. S. Soskin and M. V. Vasnetsov, "Singular optics," Prog. Opt. **42**, 219–276 (2001).
5. S. Franke-Arnold, L. Allen, and M. J. Padgett, "Advances in optical angular momentum," Laser Photonics Rev. **2**, 299–313 (2008).
6. R. Dorn, S. Quabis, and G. Leuchs, "Sharper focus for a radially polarized light beam," Phys. Rev. Lett. **91**, 233901 (2003).
7. H. Wang, L. Shi, B. Lukyanchuk, C. Sheppard, and C. T. Chong, "Creation of a needle of longitudinally polarized light in vacuum using binary optics," Nat. Photon. **2**, 501–505 (2008).
8. Q. Zhan and J. Leger, "Focus shaping using cylindrical vector beams," Opt. Express **10**, 324–331 (2002).
9. C. Varin and M. Piché, "Acceleration of ultra-relativistic electrons using high-intensity laser beams," Appl. Phys. B **74**, S83–S88 (2002).
10. L. Novotny, M. R. Beversluis, K. S. Youngworth, and T. G. Brown, "Longitudinal field modes probed by single molecules," Phys. Rev. Lett. **86**, 5251–5254 (2001).
11. A. Bouhelier, M. Beversluis, A. Hartschuh, and L. Novotny, "Far-field second-harmonic generation induced by local field enhancement," Phys. Rev. Lett. **90**, 013903 (2003).
12. F. Lu, W. Zheng, and Z. Huang, "Coherent anti-Stokes Raman scattering microscopy using tightly focused radially polarized light," Opt. Lett. **34**, 1870–1872 (2009).
13. Q. Zhan, "Trapping metallic Rayleigh particles with radial polarization," Opt. Express **12**, 3377–3382 (2004).
14. R. Oron, S. Blit, N. Davidson, A. A. Friesen, Z. Bomzon, and E. Hasman, "The formation of laser beams with pure azimuthal or radial polarization," Appl. Phys. Lett. **77**, 3322–3324 (2000).
15. Y. Kozawa and S. Sato, "Generation of a radially polarized laser beam by use of a conical Brewster prism," Opt. Lett. **30**, 3063–3065 (2005).
16. H. Kawauchi, Y. Kozawa, and S. Sato, "Generation of radially polarized Ti:sapphire laser beam using a c-cut crystal," Opt. Lett. **33**, 1984–1986 (2008).
17. X. L. Wang, J. Ding, W. J. Ni, C. S. Guo, and H. T. Wang, "Generation of arbitrary vector beams with a spatial light modulator and a common path interferometric arrangement," Opt. Lett. **32**, 3549–3551 (2007).
18. E. G. Churin, J. Hoßfeld, and T. Tschudi, "Polarization configurations with singular point formed by computer generated holograms," Opt. Commun. **99**, 13–17 (1993).
19. Z. Bomzon, G. Biener, V. Kleiner, and E. Hasman, "Radially and azimuthally polarized beams generated by space-variant dielectric subwavelength gratings," Opt. Lett. **27**, 285–287 (2002).
20. G. Machavariani, Y. Lumer, I. Moshe, A. Meir, and S. Jackel, "Spatially-variable retardation plate for efficient generation of radially and azimuthally-polarized beams," Opt. Commun. **281**, 732–738 (2008).
21. T. Fadeyeva, V. Shvedov, N. Shostka, C. Alexeyev, and A. Volyar, "Natural shaping of the cylindrically polarized beams," Opt. Lett. **35**, 3787–3789 (2010).
22. M. Stàlder and N. Schadt, "Linearly polarized light with axial symmetry generated by liquid-crystal polarization converters," Opt. Lett. **21**, 1948–1950 (1996).
23. E. Brasselet, Y. Izdebskaya, V. Shvedov, A. S. Desyatnikov, W. Krolikowski, and Y. S. Kivshar, "Dynamics of optical spin-orbit coupling in uniaxial crystals," Opt. Lett. **34**, 1021–1023 (2009).
24. L. Marrucci, C. Manzo, and D. Paparo, "Optical spin-to-orbital angular momentum conversion in inhomogeneous anisotropic media," Phys. Rev. Lett. **96**, 163905 (2006).
25. L. Marrucci, E. Karimi, S. Slussarenko, B. Piccirillo, E. Santamato, E. Nagali, and F. Sciarrino, "Spin-to-orbital conversion of the angular momentum of light and its classical and quantum applications," J. Opt. **13**, 064001 (2011).

26. E. Nagali, F. Sciarrino, F. De Martini, B. Piccirillo, E. Karimi, L. Marrucci, and E. Santamato, "Polarization control of single photon quantum orbital angular momentum states," Opt. Express **17**, 18745–18759 (2009).
27. L. Marrucci, C. Manzo, and D. Paparo, "Pancharatnam-Berry phase optical elements for wave front shaping in the visible domain: switchable helical mode generation," Appl. Phys. Lett. **88**, 221102 (2006).
28. E. Karimi, S. Slussarenko, B. Piccirillo, L. Marrucci, and E. Santamato, "Polarization-controlled evolution of light transverse modes and associated Pancharatnam geometric phase in orbital angular momentum," Phys. Rev. A **81**, 053813 (2010).
29. E. Karimi, B. Piccirillo, E. Nagali, L. Marrucci, and E. Santamato, "Efficient generation and sorting of orbital angular momentum eigenmodes of light by thermally tuned q-plates," Appl. Phys. Lett. **94**, 231124 (2009).
30. B. Piccirillo, V. D'Ambrosio, S. Slussarenko, L. Marrucci, and E. Santamato, "Photon spin-to-orbital angular momentum conversion via an electrically tunable q-plate," Appl. Phys. Lett. **97**, 241104 (2010).
31. S. Slussarenko, A. Murauski, T. Du, V. Chigrinov, L. Marrucci, and E. Santamato, "Tunable liquid crystal q-plates with arbitrary topological charge," Opt. Express **19**, 4085–4090 (2011).
32. G. Milione, H. I. Sztul, D. A. Nolan, and R. R. Alfano, "Higher-order Poincaré sphere, Stokes parameters, and the angular momentum of light," Phys. Rev. Lett. **107**, 053601 (2011).
33. A. Holleczek, A. Sztul, C. Gabriel, C. Marquardt, and G. Leuchs, "Classical and quantum properties of cylindrically polarized states of light," Opt. Express **19**, 9714–9736 (2011).
34. R. Bhandari, "Polarization of light and topological phases," Phys. Rep. **281**, 1–64 (1997).
35. E. Karimi, J. Leach, S. Slussarenko, B. Piccirillo, L. Marrucci, L. Chen, W. She, S. Franke-Arnold, M. J. Padgett, and E. Santamato, "Spin-orbit hybrid entanglement of photons and quantum contextuality," Phys. Rev. A **82**, 022115 (2010).

IOP Publishing Journal of Optics
J. Opt. **13** (2011) 064001 (13pp) doi:10.1088/2040-8978/13/6/064001

REVIEW ARTICLE

Spin-to-orbital conversion of the angular momentum of light and its classical and quantum applications

Lorenzo Marrucci[1,2], Ebrahim Karimi[1], Sergei Slussarenko[1], Bruno Piccirillo[1,3], Enrico Santamato[1,3], Eleonora Nagali[4] and Fabio Sciarrino[4,5]

[1] Dipartimento di Scienze Fisiche, Università di Napoli 'Federico II', Complesso di Monte S Angelo, 80126 Napoli, Italy
[2] CNR-SPIN, Complesso di Monte S Angelo, 80126 Napoli, Italy
[3] Consorzio Nazionale Interuniversitario per le Scienze Fisiche della Materia, Napoli, Italy
[4] Dipartimento di Fisica, Sapienza Università di Roma, Roma, Italy
[5] Consiglio Nazionale delle Ricerche-Istituto Nazionale di Ottica, Italy

E-mail: lorenzo.marrucci@na.infn.it

Received 1 December 2010, accepted for publication 18 February 2011
Published 27 April 2011
Online at stacks.iop.org/JOpt/13/064001

Abstract
A few years ago the possibility of coupling and inter-converting the spin and orbital angular momentum (SAM and OAM) of paraxial light beams in inhomogeneous anisotropic media was demonstrated. An important case is provided by waveplates having a singular transverse pattern of the birefringent optical axis, with a topological singularity of charge q at the plate center, hence named 'q-plates'. The introduction of q-plates has given rise in recent years to a number of new results and to significant progress in the field of orbital angular momentum of light. Particularly promising are the quantum photonic applications, because the polarization control of OAM allows the transfer of quantum information from the SAM qubit space to an OAM subspace of a photon and vice versa. In this paper, we review the development of the q-plate idea and some of the most significant results that have originated from it, and we will briefly touch on many other related findings concerning the interaction of the SAM and OAM of light.

Keywords: light orbital angular momentum, quantum optics, geometrical phases

(Some figures in this article are in colour only in the electronic version)

1. Introduction: spin-to-orbital angular momentum conversion

The formal separation of the angular momentum of an optical field into a spin part (SAM) and an orbital part (OAM) was first proposed by Humblet in 1943 [1]. Although a number of papers have been published on this topic since that first work (see, e.g., [2] and references therein), the problem of introducing a physically unambiguous separation of SAM and OAM of arbitrary optical fields remains still controversial and debated (see, e.g., [3–8]). Nevertheless, such a separation becomes clearly unambiguous and physically meaningful in the paraxial limit [9]. A paraxial beam has a well defined SAM that is associated with its circular polarization content. The OAM, however, can be further split into two components [10]: (i) an external one, that arises from the cross product of the total momentum transported by the beam and the position of its axis relative to the origin of coordinates; (ii) an internal OAM component that is associated with the helical structure of the optical wavefront around the beam axis and with an optical

vortex located at the beam axis [9]. The internal OAM acts as a sort of additional spin of the whole beam around its axis, as it is always oriented parallel to the beam axis and it is independent of the choice of the origin of coordinates. However, while the SAM per photon can only take two values, namely $S_z = \pm\hbar$, where $\hbar$ is the reduced Planck constant and z is the beam axis, the OAM per photon can be any positive or negative integer multiple of $\hbar$, i.e., $L_z = m\hbar$ with m any integer. The integer m also defines the phase variation of the optical beam seen when circling its axis, i.e., the wavefront phase factor $\exp(im\varphi)$, where φ is the azimuthal angle around the optical axis z. The spin and orbital angular momentum components can also be distinguished according to their different mechanical actions on small absorbing particles, with the SAM inducing spin of the particle independent of its position, while the OAM induces revolution of the particle around the beam axis [11, 12, 10]. The possibility of distinguishing between SAM and OAM according to their coupling with different rotational degrees of freedom of optical media has also been considered [13].

Since SAM is associated with optical polarization and OAM with the optical wavefront, at first sight they appear to be quite separate and non-interacting properties of light, at least in the paraxial limit. For this reason, for about ten years after the publication of the seminal paper by Allen *et al*, which started the current field of research in the optical OAM, the possibility of an interaction between SAM and internal OAM taking place in a single paraxial optical beam was not considered. The generation and control of optical OAM has been based only on essentially polarization-independent tools, such as cylindrical lenses [9], spiral phase plates [14], holograms [15–17] (including reconfigurable ones made using spatial light modulators), and Dove prisms, also in suitable interferometric setups [18, 19].

In 2002, following an original idea by Bhandari [20], the group of Hasman in Technion University reported the use of patterned subwavelength diffraction gratings for reshaping the wavefront of an electromagnetic wave, so as to obtain various wavefronts, including helical beams [21, 22]. The underlying concept was that of manipulating the beam polarization so as to introduce a space-variant Pancharatnam–Berry phase. For this reason, these phase devices were called Pancharatnam–Berry optical elements (PBOE). Subwavelength grating PBOEs were however experimentally demonstrated only for mid-infrared electromagnetic waves, due to manufacturing limitations (subwavelength grating PBOEs working in the near-infrared have been reported only recently [23]). In 2006, Marrucci *et al* (initially unaware of Hasman's work) proposed that anisotropic inhomogeneous media such as liquid crystals could give rise to a previously unrecognized optical process in which the variation of SAM occurring from the medium's birefringence gives rise to the appearance of OAM, arising from the medium's inhomogeneity [24]. In rotationally symmetric geometries, this process involves no net transfer of angular momentum to matter, so that the SAM variation in the light is entirely converted into its OAM. For this reason, the process was dubbed 'spin-to-orbital conversion of angular momentum' (STOC). Marrucci *et al* also demonstrated this process experimentally with visible light, by using patterned liquid crystal cells that were called 'q-plates' [24, 25]. The first demonstration of the STOC process for single photons and photon pairs was reported a few years later by Sciarrino and co-workers [26].

This advance did not arise out of the blue. The Naples optics group had been working on the exchange of angular momentum of light with anisotropic media such as liquid crystals (including puzzling enhancement effects arising when the liquid crystals are doped with certain dyes) since the mid 1980s (see, e.g., [27–32, 13]). The STOC process idea actually sprung from the observation that radially oriented liquid crystal droplets trapped into circularly polarized laser beams did not rotate [33], and from the ensuing question, asked by Jánossy, about the fate of the spin optical angular momentum in such a process. The conceptual answer provided by the STOC idea has been subsequently directly demonstrated in a later experiment performed just with liquid crystal droplets [34]. A detailed analysis of the torques and forces arising in a liquid crystal droplet by the effect of the interaction with light was later reported by Jánossy [35].

The q-plate was first conceived as a 'simplified' (flattened) liquid crystal droplet. In a more general definition, a q-plate is a slab of a birefringent material, e.g., a liquid crystal, having a uniform birefringent phase retardation δ and a transverse optical axis pattern with a nonzero topological charge. The pattern is defined by the number q of rotations that the optical axis exhibits in a path circling once around the center of the plate, where a topological defect must be present (q is negative if the direction of the axis rotation is opposite to that of the path). The number q must clearly be integer or semi-integer, since the optical axis has no polarity. q is also the charge of the topological singularity located at the center of the plate. A secondary parameter defining the q-plate pattern is the initial optical axis orientation, as for example specified by the angle α_0 it forms at a reference angular position in the transverse plane (e.g., on the x axis in the plate). Some examples of q-plate patterns are shown in figure 1.

For $\delta = \pi$, i.e. at so-called optimal tuning, a q-plate modifies the OAM state m of a circularly polarized light beam passing through it, imposing a variation $\Delta m = \pm 2q$ whose sign depends on the input polarization, positive for left-circular and negative for right-circular. The handedness of the output circular polarization is also inverted, i.e. the SAM is flipped. In other words, a q-plate gives rise to a polarization-controlled variation of OAM. In particular, in the rotationally symmetric case $q = 1$, the OAM variation balances the SAM one, so that the total angular momentum of the light beam is conserved, and we have a pure STOC process. This behavior is pictorially illustrated in figure 2. An untuned q-plate with $\delta \neq \pi$ will give rise to a superposition of a wave transformed just as for the tuned case and an unmodified wave, with amplitudes respectively given by $\sin(\delta/2)$ and $\cos(\delta/2)$. These optical properties of the q-plate can be simply derived using the Jones matrix calculus, valid in the limit of negligible transverse diffraction inside the q-plate (i.e., very thin q-plates) [36].

A tuned q-plate allows one to generate a pure helical beam carrying nonzero OAM (with $m = \pm 2q$) starting with a circularly polarized Gaussian input mode (having $m = 0$),

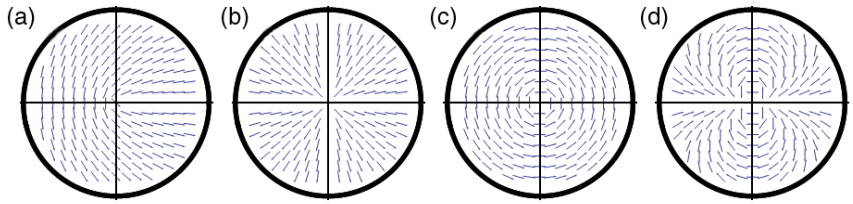

Figure 1. Four examples of q-plate patterns. (a) $(q, \alpha_0) = (\frac{1}{2}, 0)$, (b) $(q, \alpha_0) = (1, 0)$, (c) $(q, \alpha_0) = (1, \frac{\pi}{2})$ and (d) $(q, \alpha_0) = (2, 0)$. The segments indicate the optical axis orientation in the transverse plane.

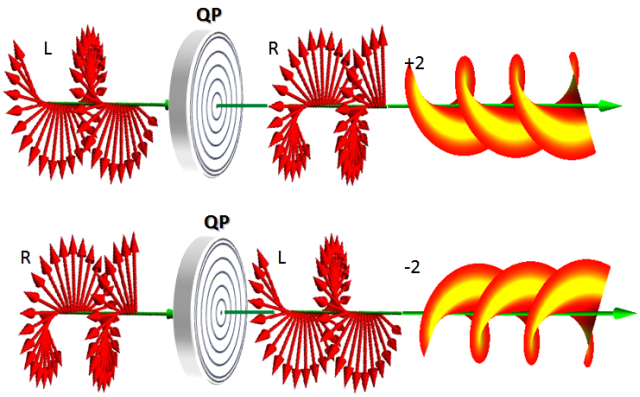

Figure 2. Pictorial illustration of the optical action of a tuned q-plate on an input circularly polarized plane-wave light, for the case $q = 1$. The output is a helical mode with OAM given by $m = \pm 2$, with the sign determined by the input polarization handedness.

with very high efficiency (ideally close to 100%), no deflection of the propagation axis and with a polarization-controlled handedness [37, 38]. q-plates can therefore provide a very convenient approach to generating OAM beams, which can compete with computer-generated holograms and spatial light modulators. The polarization control of the OAM sign allows high-speed switching with rates that in principle can reach GHz values [25]. Even more interestingly, the polarization control of the OAM sign allows the development of new kinds of quantum manipulations of single photons, as has been demonstrated in a series of experiments mainly performed by Sciarrino and co-workers in Roma's quantum optics group, which will be reviewed below. In particular, as we will show, the combined use of polarization and OAM for accessing a high-dimensional quantum space attached to each photon is progressively enabling the implementation of novel promising quantum information protocols [39, 40].

Inhomogeneous birefringent media such as q-plates are not the only systems in which STOC can take place. An inhomogeneous dichroic medium, such as a space-variant polarizer with a q-plate-like optical axis geometry, can give rise to very similar phenomena (with the advantage of an achromatic response and the disadvantage of significant optical losses) [41]. An electro-optical device allowing a polarization-controlled OAM manipulation quite similar to the q-plate one, based on a pair of opposite spiral phase plates having electrically controlled refractive index, has been theoretically proposed recently [42]. A STOC phenomenon bearing many similarities to that taking place in a q-plate with $q = 1$ may also occur in a homogeneous uniaxial birefringent crystal, when an optical beam propagates along the optical axis of the crystal. This was first proved theoretically by Ciattoni *et al* [43, 44] and experimentally by Brasselet *et al* [45–47]. A similar phenomenon has been shown to occur in a biaxial crystal by internal conical diffraction [48, 49]. In contrast to the case of q-plates, however, this approach is limited to generating OAM $m = \pm 2$, due to the rotational symmetry of the medium. Moreover, the conversion efficiency in the paraxial limit cannot be higher than 50%. Another interesting situation in which a form of STOC takes place is when an initially paraxial circularly polarized beam passes through a short-focal-length lens. The resulting strongly-focused non-paraxial beam exhibits an OAM content, as demonstrated experimentally by particle manipulation experiments [50, 51]. In this case, however, the OAM per photon remains small and its effects are clearly visible only close to the beam focus. The possibility of an electro-optical modulation of this effect has also been reported [52]. Another recent work showed that optical beams having a radially varying SAM also acquire an additional rather unexpected component of OAM-like angular momentum, presumably arising as a consequence of departure from the paraxial limit [53].

Moreover, the interaction of SAM and external OAM, that is at the basis of the so-called optical spin Hall effect, has also been recently conceived and experimentally demonstrated [54, 55]. Related spin–orbit optical phenomena are the polarization 'geometrodynamics' [56, 57] and the polarization-based optical sensing of nano-particle displacements [58]. It should be furthermore mentioned that several works in the field of singular optics [59], that is strictly related with that of OAM, have recently tackled issues concerning the interaction between polarization and wavefront structures in the optical field (see, e.g., [60–62]). Finally, an emerging field in which the spin–orbit interaction of SAM and OAM may bear fruitful results in the near future is that of optical polariton condensates in semiconductor microcavities (see, e.g., [63, 64]).

In the rest of this paper, we discuss some of the main developments that have arisen since the first introduction of the q-plate and the observation of the STOC process. The paper is organized as follows. In section 2 we survey the developments in the technology for manufacturing and tuning the liquid crystal q-plates and mention some nonlinear phenomena in which a q-plate-like geometry takes place spontaneously. Section 3 concerns the theory of optical propagation inside a q-plate and the resulting optical modes at the q-plate output. Section 4 is mainly about the optical setups for

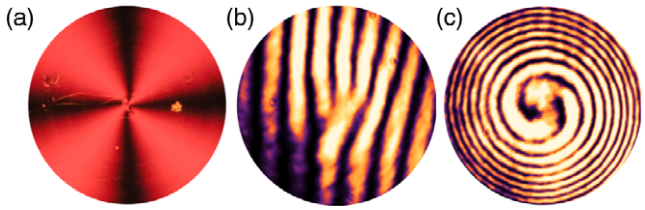

Figure 3. (a) A $q = 1$ q-plate prepared by a photoalignment technique, as seen between crossed polarizers. (b), (c) Interference patterns of the outgoing beam from the q-plate with (b) planar and (c) spherical reference waves, for a left-circular input polarization.

OAM manipulation that can be obtained by combining one or more q-plates in suitable optical schemes, but it includes a brief survey of related results of polarization-based OAM manipulation. Quantum applications of q-plates and of SAM–OAM photon interactions are finally discussed in section 5.

2. q-plate manufacture and tuning

The main issue to be addressed in the manufacture of q-plates is the patterning of the optical axis. Liquid crystals (LCs) are soft birefringent materials allowing flexible spatial patterning of the average molecular orientation that defines the optical axis. LCs can be aligned by several methods. For static alignment, the simplest choice is to use the so-called 'surface anchoring', i.e., a treatment of the bounding substrates that generates a preferential molecular alignment of the LC in contact with the surface. For dynamical alignment one can use external fields, such as magnetic, electric or even optical fields. LC q-plates can be then manufactured as thin (order of 5–10 μm) LC films, sandwiched between two glass substrates which have been previously coated with a suitable alignment layer, typically made of polymer, such as polyimide or other materials. These materials are suitable for aligning the LC optical axis parallel (or slightly tilted) to the bounding surfaces, i.e. the so-called 'planar anchoring'. To single out a specific direction in the plane one can then use a mechanical rubbing procedure (using velvet or other fabrics) of the polymer-coated substrate. It is, however, hard to introduce an arbitrary pattern by mechanical rubbing, and this approach is convenient only in the case of the simplest geometry, corresponding to $q = 1$, which is rotationally symmetric. For this practical reason all the early experimental works with q-plates used q-plates with $q = 1$.

A more versatile and cleaner approach to patterning LC cells is to use a photoinduced alignment method of the polymer coating of the LC-bounding substrates, as proposed in [25]. In this approach, the anisotropy of the polymer is controlled by the linear polarization of the writing light, which defines the material optical axis (either parallel or perpendicular to the writing field polarization). There are different permanent orienting effects of light on the polymer coatings which can be used. The most common ones are either photochemical, i.e. based on selectively destroying or creating chemical links by preferential absorption, or photophysical, i.e. based on the photoinduced selective reorientation of dye molecules dispersed in the polymer. One can use this

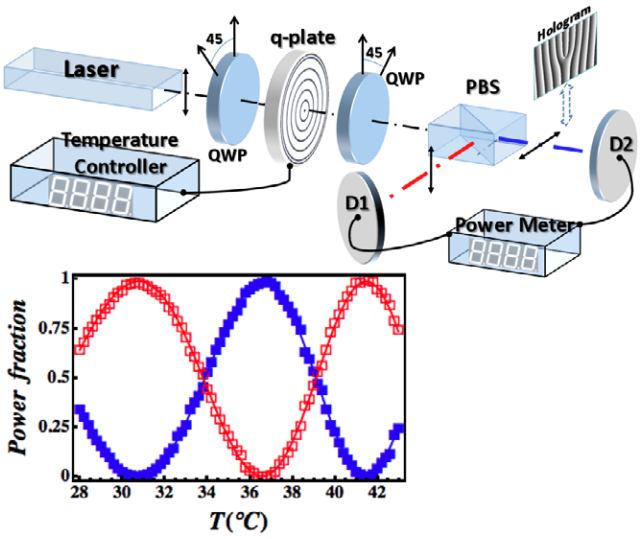

Figure 4. Setup used to measure the STOC efficiency and the state purity. Legend: QWP—quarter wave plate, PBS—polarizing beam-splitter. The fork hologram was inserted on the converted beam arm to verify the degree of purity of the OAM $m = 2$ mode generated on the output. STOC power fraction (blue ■) and no STOC power fraction (red □) as functions of the q-plate temperature. The curves are theoretical best fits [38].

approach to directly write an anisotropic pattern in a thin polymer film that becomes itself a q-plate, as for example recently reported in [65]. However, polymer q-plates are not dynamically tunable, as their birefringent retardation δ is fixed by the film thickness and by the polymer degree of alignment and corresponding birefringence. We instead recently demonstrated the photoinduced alignment approach to prepare patterned polymer-coated substrates with which we could assemble tunable patterned LC q-plates with arbitrary topological charge q [66]. In figure 3 an LC q-plate manufactured by the photoalignment method is shown, together with the interference patterns demonstrating the helical structure of the outgoing wavefront.

The tuning of an LC q-plate, that is controlling the birefringence phase retardation δ, useful for optimizing the STOC process or to adjust it for different wavelengths, can be achieved by different methods, including mechanical pressure, thermal methods, and external-field induced LC reorientation. So far, a thermal approach exploiting the strong dependence of the LC birefringence on temperature [38] and an electric one, exploiting the electric-field induced reorientation of the LC molecular alignment [67] have been demonstrated. The latter of course allows for a relatively fast dynamical control of tuning, while the former is more suitable for static tuning.

Since the STOC process is accompanied by polarization helicity inversion, in the case of a pure circularly polarized input beam the STOC and non-STOC components of the output light can be simply separated by a polarizing beam-splitter (PBS), because the converted and non-converted light will have orthogonal polarization states. This allows for a very simple measurement of the STOC efficiency and of the phase retardation δ that controls it, as shown for example in figure 4. In this experiment, the optimal STOC efficiency exceeded

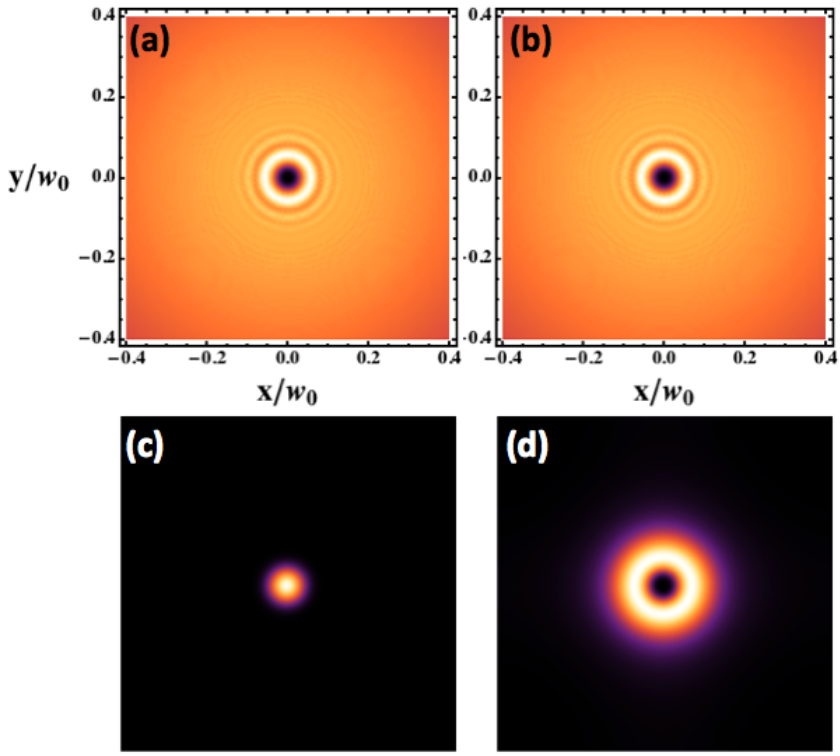

Figure 5. Intensity profile at the exit face of the $q = 1$ q-plate. (a) No SAM-to-OAM conversion; (b) full SAM-to-OAM conversion. Intensity profile in the far-field beyond the q-plate. (c) No SAM-to-OAM conversion; (d) full SAM-to-OAM conversion [37]. A circularly polarized TEM_{00} input beam has been assumed.

99%, neglecting reflection and diffraction losses (85% taking into account losses, which, however, were not minimized with anti-reflection coatings).

Before concluding this section, we should mention that certain light-induced modifications of materials, for example associated with thermal-induced stresses [68, 69], as well as nonlinear optical phenomena, such as those taking place in LCs themselves in suitable geometries [70, 71], have been shown to be capable of spontaneously generating q-plate-like structured media, thus giving rise to STOC phenomena, although usually not with very high conversion efficiency. In such cases, the STOC concept provides anyway a convenient framework for revealing and analyzing the associated optical effects.

3. Optical propagation through q-plates and outgoing modes

The simplest theory of optical propagation through the q-plate is based on the assumption that at each transverse position x, y the propagation is independent (as for a local plane wave), which corresponds to the geometrical optical approximation. The only effect of the birefringence is then that of altering the polarization and introducing a Pancharatnam–Berry phase, as can be derived using a simple Jones matrix approach. This simple theory, proposed in the early papers [24, 25, 72, 36], neglects any transverse diffraction effects arising in the propagation. This is certainly a very good approximation in the limit of thin q-plates and wide beams, but not applicable for points that are very close to the central singularity, where the rapid transverse spatial variations associated with the singularity are expected to give rise to significant diffraction effects.

To go beyond the geometric-optical approximation, one needs to model the diffraction of the helical waves traveling in the q-plate and emerging from it. Being helical, such modes are often simply referred to as Laguerre–Gauss (LG) modes. However, while the azimuthal phase factor of the helical modes is always just the same as for a pure LG mode, their radial structure may be different, and in general one can only say that helical modes can be written as superpositions of LG modes having different radial index p and the same azimuthal index m. It can be shown that for an ideally thin q-plate, as well as for any spiral phase plate, the outgoing modes obtained in the paraxial limit, when at input there is a pure TEM_{00} Gaussian mode, form a subset of a general class of modes that has been recently introduced, the 'hypergeometric-Gaussian modes' [73].

These same modes are also useful for describing the propagation inside the q-plate. An approximate analytical solution of this problem, exploiting the q-plate symmetry in the limit of high beam paraxiality, was proposed in [37]. The radial profile of the optical beam at any transverse plane z inside the q-plate (or at the output face) is found to be independent of the cumulated birefringent optical retardation at z and can be given in terms of superposition of two ordinary and extraordinary hypergeometric-Gaussian modes. As a consequence, the intensity patterns of the outgoing beams of a tuned or detuned q-plate in the near-field are identical. Nevertheless, in the far-field, the Gaussian or doughnut shapes of the intensity profile will reemerge depending on the OAM, as is shown in figure 5.

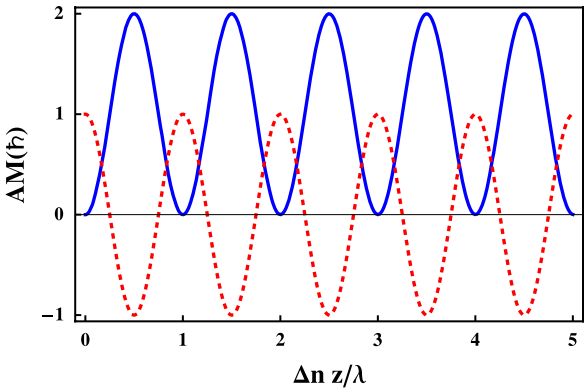

Figure 6. OAM (blue solid line) and SAM (red dotted line) as a function of the optical retardation $\Delta nz/\lambda$ for a thin $q = 1$ q-plate. The input beam is left-circularly polarized TEM_{00}. We have assumed the following data: LC refractive ordinary and extraordinary indices $n_o = 1.5$ and $n_e = 1.7$, respectively, and beam waist $w_0 = 50\lambda$.

The cumulated optical retardation of the plate controls the SAM-to-OAM conversion, or STOC, as shown in figure 6. Compared with the geometric-optical approximation, this more exact theory predicts a very slow decrease of the optimal efficiency with increasing q-plate thickness, due to internal diffraction.

An exact vectorial theory of rotationally symmetric Bessel beams propagating in q-plates with $q = 1$ and of the associated STOC phenomenon has also been reported [74]. An interesting analogy with the Aharonov–Bohm effect for the propagation of light in a nematic liquid crystal with a disclination, corresponding to a q-plate geometry, has been proposed by Carvalho *et al* [75].

4. Manipulation of azimuthal modes via polarization

The q-plate and the resulting SAM–OAM coupling and STOC process have provided the basis for several novel optical devices and setups for manipulating the OAM of light. Many of these devices, although they are essentially classical, find a natural important application in the quantum information setting, so we will come back to them in the following section.

An important concept is the one-to-one mapping that can be established between the space π of all possible (generally elliptical) polarization states and an arbitrary two-dimensional subspace of the OAM degree of freedom, spanned by two opposite OAM values $m = \pm\ell$, hereafter denoted as o_ℓ. This subspace is defined independently of the radial mode (this is for example appropriate if the radial mode is separable and can be factorized). Both π and o_ℓ spaces are two-dimensional complex vector spaces having the same structure as the Hilbert space of a quantum spin, or as the representations of the SU(2) group. Neglecting a global phase, any point in such a space can be represented as a point on a three-dimensional sphere, the Poincaré sphere in the case of polarization, or an analogous sphere in the OAM case [76] (both being analogous to Bloch's sphere used for quantum spins). An arbitrary state in an OAM o_ℓ subspace is generally not a pure helical beam, but it can always be written as the superposition of the two opposite

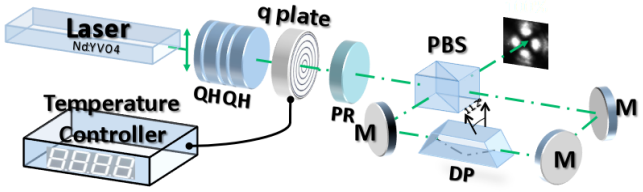

Figure 7. Scheme of an experimental setup based on a q-plate and a Dove prism in a polarizing Sagnac interferometer, that allows for 100%-efficient transfer of an arbitrary SAM-encoded input state into an OAM bi-dimensional state, or vice versa. Legend: QHQH—set of waveplates to generate an arbitrary polarization state; PR—polarization rotator; PBS—polarizing beam-splitter; DP—Dove prism; M—mirror [78].

OAM basis states. This is just the same as for the polarizations, which in general are not associated with well defined values of the photon SAM, but can always be decomposed into a superposition of the two circularly polarized waves with opposite handedness.

Now, a q-plate in combination with other optical devices allows one to physically implement just this mapping. There are both unitary and non-unitary schemes. The non-unitary schemes waste a fraction of the input optical energy (i.e., they are 'probabilistic', in the language of quantum information, because a fraction of the photons are lost). However they can be very simple. For example, a single q-plate followed by a linear polarizer allows one to transfer the polarization input state into the corresponding OAM subspace o_ℓ with $\ell = 2q$ [77]. This scheme, however, has a 50% efficiency (or success probability). The opposite transfer, from OAM to SAM, can be obtained by combining a q-plate with a single-mode fiber, used for filtering $m = 0$ states [77]. This is again a scheme with 50% efficiency.

A 100% efficient mapping, that is a unitary scheme, can be obtained by combining a q-plate and one or two Dove prisms inserted into an interferometer, such as a Mach–Zehnder or (more conveniently) a Sagnac [77, 78]. This scheme, illustrated in figure 7, is fully reciprocal and can therefore work in both directions (see also [79] for another proposed optical scheme, not based on the q-plate, in which the OAM state is controlled by polarization via a Sagnac interferometer). This scheme was demonstrated experimentally in the classical regime [78]. An additional feature of this setup is that also the geometrical Pancharatnam–Berry phase arising from the polarization manipulations is transferred to the OAM output beam. Examples of the resulting modes on the OAM-Poincaré sphere for $\ell = 2$ are given in figure 8. The interference fringes with a reference beam, also shown, were used to analyze the output mode phase structure and to measure the geometric phase.

It must be emphasized that this setup can generate a class of azimuthal transverse modes, including all modes that have the same azimuthal structure as the Hermite–Gaussian modes, with a theoretical efficiency of 100%. The choice of the generated mode is entirely controlled by the input polarization, which can be manipulated at very fast rates. This should be contrasted with the more limited efficiency of the spatial light

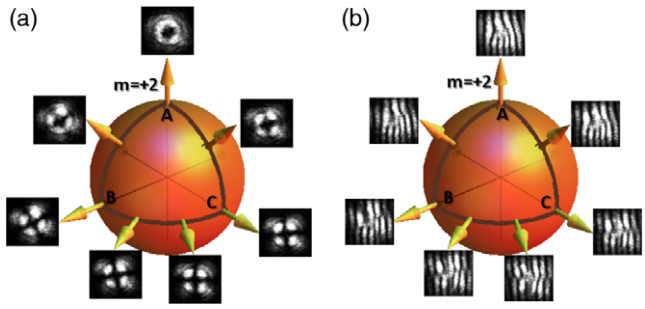

Figure 8. A possible closed path over the OAM-Poincaré sphere. The path starts and ends at the pole. (a) Intensity profiles of the generated beam at different points of the path. (b) Corresponding interference patterns with a TEM_{00} linearly polarized reference beam [78].

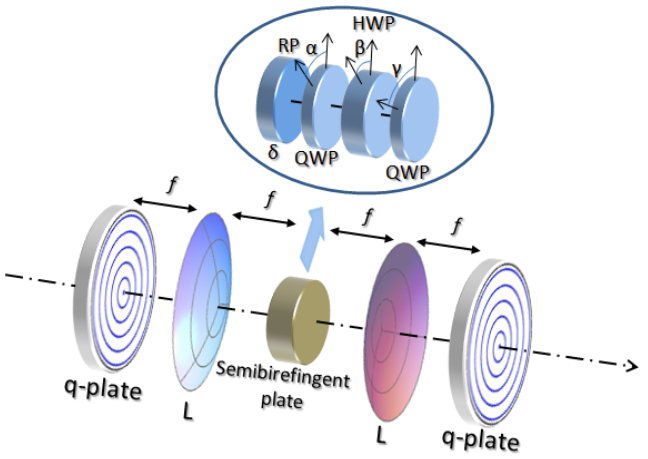

Figure 9. A scheme of a q-box. A SAM (polarization) unitary gate is shown in the inset [81]. Legend: QWP—quarter wave plate, HWP—half wave plate, L—lens, RP—retardation plate.

modulators (typically below 70%) and slow response (less than 1 kHz). The possibility of controlling even a four-dimensional OAM subspace, including both $m = \pm 2$ and ± 4 states, by a single q-plate inserted in an optical loop scheme has also been reported very recently [80].

A different optical scheme, still based on the q-plate, can be used as a spin–orbit SAM–OAM four-dimensional mode sorter and detector [38]. The four-dimensional space is the tensor product of the polarization space π and an OAM subspace o_ℓ. In other words, arbitrary optical states are defined as linear combinations of four basis states $|L, \ell\rangle$, $|L, -\ell\rangle$, $|R, \ell\rangle$ and $|R, -\ell\rangle$, where L, R denote the left- and right-circular polarizations. The sorting is based on two steps. First, there is a q-plate-induced shifting of the OAM value of the beam. Assuming that the input beam has an OAM given by the number $m = \ell$ (in units of $\hbar$), the q-plate will convert it into either $m = 0$ or 2ℓ, depending on the input polarization handedness. This requires using a q-plate with $q = \ell/2$ (in the reported experiment, $q = 1$ and $\ell = 2$ were used). Next, the beam is split according to the outgoing circular polarization and further separated by radial sectioning, e.g. by using a mirror with a hole to reflect only the external doughnut component and let the central spot pass. This radial sectioning exploits the coupling between the OAM and the radial profile that emerges during free propagation. The small residual overlap of the two radial modes, however, gives rise to a non-perfect contrast ratio. The contrast ratio can be improved without limitations at the expense of detection efficiency by blocking the annular region where mode overlap occurs.

The last device that we mention in this section was proposed to perform arbitrary unitary transformations in the spin–orbit four-dimensional space $\pi \otimes o_\ell$, keeping always the single-beam structure (i.e., without splitting the beam into an interferometer scheme) [81]. It is based on a complex combination of q-plates, birefringent waveplates and lenses, and it again exploits the coupling between the radial mode and the OAM arising in the free propagation. This setup was proposed mainly with quantum applications in mind, as it provides a universal quantum gate for the spin–orbit Hilbert space of a single photon. But being a single photon device it can be also discussed as a classical optics device, so we discuss it here.

The working principle of this device is similar to that of the spin–orbit mode sorter just described, as it exploits the spatial separation of the $m = 0$ and 2ℓ modes occurring in the radial coordinate in the free propagation. An important element is the so-called 'q-box' (QB), which is made of two q-plates and a unitary polarization gate sandwiched between them (which is essentially a combination of suitable waveplates and isotropic phase retardation plates). The radius of the waveplates of the spin gate is selected so to act only on the $m = 0$ mode, leaving the $m = 2\ell$ one unchanged. The propagation-induced coupling between the OAM and the radial coordinate is controlled by suitable lenses to switch between near-field and far-field and back. A schematic illustration of the q-box device is given in figure 9. A sequence of four q-boxes separated by quarter and half waveplates (QWP and HWP) in the following order: QB → QWP → QB → HWP → QB → QWP → QB will make a 16-parameter unitary gate that will correspond to a 4×4 unitary matrix which is universal, meaning that by adjusting the parameters one can realize any unitary operation on the spin–orbit optical state. Such a highly complex setup, however, is not always necessary. Many important gates can be realized with many fewer elements. For example, the CNOT gate can be realized with a single q-box having a single half wave plate inside.

Because of the presence of residual overlaps of $m = 0$ and 2ℓ modes in the radial coordinate, the fidelity of the q-box is not 100%. An optimal selection of the radius of the waveplates in the q-box can provide a minimum fidelity of about 83% for $\ell = 2$ (but the fidelity increases if higher order OAM modes are considered and it can become close to 100% for specific input–output states). As for the mode sorter, the fidelity can be increased at the expense of efficiency (success probability in the quantum applications) by stopping the annular regions where the overlap takes place.

5. Quantum information applications: qubits and qudits in spin–orbit states

The interest of the OAM degree of freedom of light in the quantum information field [82] mainly arises from the

possibility of using its high-dimensionality for encoding a large amount of information in single photons and from the robustness of such encoded information due to the angular momentum conservation law [2, 83]. The standard unit of quantum information is the qubit, a two-dimensional quantum state. OAM allows the encoding of qubits by exploiting any two-dimensional subspace, such as the o_ℓ ones or others. However, many quantum information protocols benefit from the use of so-called 'qudits', that are higher-dimensional quantum states, for encoding the information. OAM provides an obvious possibility for qudit optical implementation, by exploiting a larger subspace. Moreover, OAM can be readily combined with other degrees of freedom of the photon in order to further expand the Hilbert space or to realize the so-called hyper-entanglement, where different degrees of freedom of two particles are simultaneously entangled [84, 85]. In particular, the combination of OAM with SAM is of special interest here, given the similar nature of the two degrees of freedom and given the possibility, offered by devices such as the q-plate, of coupling and manipulating the two degrees of freedom together. Another interesting potential application of combining SAM and OAM is to create a frame-invariant encoding of quantum information [86, 87].

The action of a q-plate on a single photon quantum state is essentially the same as for the fields of classical coherent light. Let us introduce the ket notation $|P, m\rangle = |P\rangle_\pi |m\rangle_o$ for the single photon states, where P stands for the polarization state (e.g., $P = $ L, R, H, V for left- and right-circular polarizations and horizontal and vertical linear polarizations) and m is the OAM value in units of $\hbar$. The radial state is omitted for brevity (this is possible when the radial state can be factorized out). The q-plate action (here, and in the following, optimal tuning is assumed), which can be associated to a quantum evolution operator $\widehat{\mathrm{QP}}$, is then described by the following rules:

$$\begin{aligned} \widehat{\mathrm{QP}}|L\rangle_\pi |m\rangle_o &= |R\rangle_\pi |m + 2q\rangle_o \\ \widehat{\mathrm{QP}}|R\rangle_\pi |m\rangle_o &= |L\rangle_\pi |m - 2q\rangle_o. \end{aligned} \tag{1}$$

When applied to an input linearly polarized light (e.g., horizontal) having $m = 0$, we obtain the following output state:

$$\widehat{\mathrm{QP}}|H\rangle_\pi |0\rangle_o = \frac{1}{\sqrt{2}} \left(|L\rangle_\pi |-2q\rangle_o + |R\rangle_\pi |2q\rangle_o\right). \tag{2}$$

The right-hand-side expression can be interpreted as an entangled state of the SAM (or polarization) and OAM degrees of freedom of the same photon (of course this kind of single-particle entanglement does not involve non-locality effects). These predictions have been tested experimentally on heralded single photon states obtained by spontaneous parametric down-conversion (SPDC) [26].

An interesting application of the q-plate is for realizing optical devices that can transfer the quantum information initially stored in the polarization degree of freedom of the photon into the OAM degree of freedom, or vice versa. In other words, these devices may implement the following transformations (in both directions):

$$|\psi\rangle_\pi |0\rangle_o \leftrightarrows |H\rangle_\pi |\psi\rangle_o \tag{3}$$

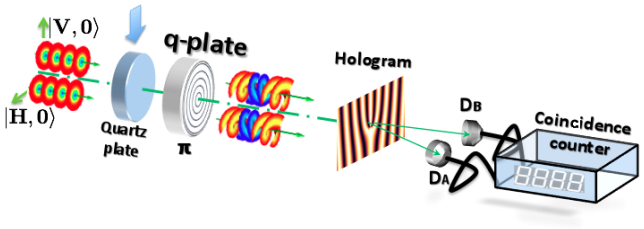

Figure 10. The schematic of the biphoton OAM coalescence setup. The SPDC source generates pairs of correlated photons having H and V polarizations. The q-plate converts this correlation in the OAM space. The correlations can then be tested by the vanishing coincidence measurements on opposite OAM states, as filtered using a fork hologram. A quartz plate can be used to introduce a delay between the two input photons, thus destroying the quantum correlations [26].

where $|\psi\rangle$ here stands for an arbitrary qubit state and we have chosen to use $|H\rangle_\pi$ as the 'blank' state of polarization and $|0\rangle_o$ as the blank state of OAM (other choices are obviously possible). These quantum information transfer devices can be implemented either probabilistically or deterministically, by adopting the optical schemes presented in [26, 77, 88] and experimentally verified in the simpler probabilistic schemes within the heralded single photon regime. These experiments showed a quantum fidelity of 97% or higher. Multiple SAM $\rightarrow$ OAM $\rightarrow$ SAM and cascaded SAM $\rightarrow$ OAM $m = |2| \rightarrow$ OAM $m = |4|$ transfers were also demonstrated [77].

The single photon manipulations discussed above, although performed in the heralded mode ensuring the presence of one and only one photon at a time, are not truly different from classical optics experiments (such as those discussed in section 4). Uniquely quantum effects that cannot be explained with classical theories only arise when dealing with more than one particle. The generation of a biphoton state with nontrivial OAM quantum correlations was demonstrated in [26], again using a q-plate. The experiment is illustrated in figure 10. A biphoton state is a single optical mode having exactly two photons. In the reported experiment, a biphoton state having polarization correlations was initially generated by SPDC, and the SAM–OAM transfer device was then used to generate the final state with OAM correlations. It must be noted that the q-plate acted on the two photons simultaneously in this experiment. Such action cannot be described in classical terms. After erasing the polarization degree of freedom, the biphoton state finally generated can be described as follows [26]:

$$\frac{1}{\sqrt{2}} \left(|+2\rangle_o |+2\rangle_o + |-2\rangle_o |-2\rangle_o\right) \tag{4}$$

where the OAM values were in the subspace with $\ell = 2$ because the employed q-plate had $q = 1$. The successful generation of this state can be verified by testing for OAM correlations occurring when detecting two-photon coincidences. In particular, a vanishing number of counts is expected when testing for coincidences between opposite values of the OAM. The coincidence counts are instead restored if the two photons are delayed, e.g. by inserting a

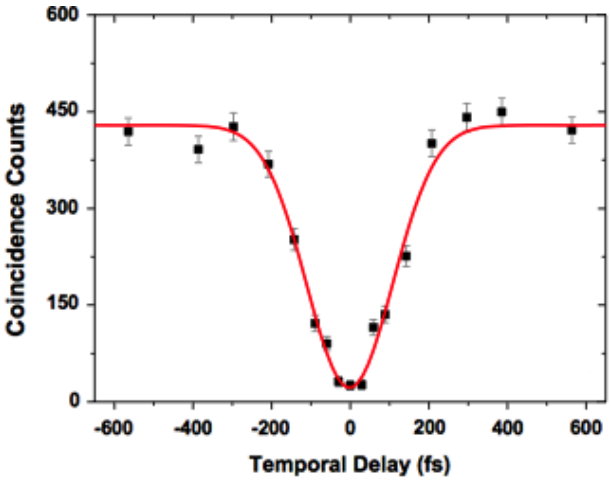

Figure 11. Coincidence counts obtained in the measurement of opposite OAM values for the biphoton generated by the q-plate, as illustrated in figure 10.

suitable birefringent crystal such as a quartz plate, so as to become distinguishable. A typical 'coincidence dip' behavior is therefore observed, as shown in figure 11. Other tests on the biphoton state, including a verification of the enhanced coalescence probability in OAM and a test of coherence based on analyzing the two photons in OAM-superposition states by suitable holograms, have also been performed. We refer the reader to [26] for further details.

Thanks to the SAM–OAM quantum transfer devices, an arbitrary qubit photon state can be initially prepared in the SAM space and then transferred into the OAM space. Any OAM state can also be conveniently analyzed by simply transferring it back to the SAM space. This makes the OAM utilization in quantum photonic experiments much easier than it was before. This technology step has, for example, allowed the first experimental demonstration of Hong–Ou–Mandel (HOM) coalescence [89] of OAM-carrying photons in a beam-splitter [90]. This phenomenon results from the two-photon interference between the photons impinging on a beam-splitter from two different input ports. Such interference, due to the bosonic nature of photons, leads to a doubled probability for the two photons to emerge together from the same output port of the beam-splitter and a vanishing probability for the two photons to emerge from the two separate output ports. This works only when the two photons are indistinguishable, i.e. the impinging wavepackets are synchronous and the SAM and OAM states of the two photons are the same (after taking into account the reflection inside the beam-splitter). This behavior was well demonstrated in the experiment [90]. The importance of this proof-of-principle demonstration is that the HOM coalescence effect is an enabling process, on which many other quantum information protocols are based (such as quantum teleportation, quantum cloning, etc). And, indeed, in the same paper the implementation of optimal quantum cloning of OAM-encoded photonic qubits was also demonstrated [90].

Transfer devices have also recently enabled the preparation of spin–orbit hybrid-entangled photons [91, 92]. Two opposite approaches have been demonstrated. By starting with a polarization (SAM) entangled pair generated by SPDC, one can transfer the quantum information of only a single photon of the pair from SAM to OAM to obtain the hybrid entanglement [91]. Conversely, by starting with an OAM entangled pair (also generated by SPDC, as first demonstrated in [93]), it is possible to reach the hybrid entanglement by an OAM-to-SAM quantum transfer [92]. In these works, the entanglement has been confirmed by testing the violation of a Bell's inequality [91, 92, 94]. The non-separability (or single-particle entanglement) of SAM and OAM degrees of freedom has also been investigated, using q-plates or interferometric layouts, both in a classical intense beam regime [95, 92] and in a heralded single photon one [26, 96, 94, 92]. The remote preparation of single-particle hybrid-entangled states has also recently been demonstrated (not using q-plates), by exploiting an SAM–OAM hyper-entangled photon pair source [97]. A proposal for hybrid entanglement multi-photon manipulations exploiting the q-plate has also recently been put forward [98].

Finally, the most recent progress in the use of SAM–OAM coupling for quantum information has been based on combining both degrees of freedom for encoding qudits. Even though some implementations of quantum states with dimension higher than two have already been carried out with biphoton states [100–103], an appealing goal is that of encoding as much information (i.e. as many qubits) as possible in a single photon by exploiting different degrees of freedom, so as to exceed the limitations due to noise interactions. In particular, by encoding a qubit in SAM and another qubit in an OAM subspace one obtains a single photon 'ququart', i.e. a quantum state with dimension $d = 4$ defined in the Hilbert space $\pi \otimes o_l$. The preparation and measurement of single photon ququarts by using a q-plate based apparatus was demonstrated in [104]. Interestingly, in this work all states belonging to the five mutually unbiased bases that span the four-dimensional Hilbert space were generated and measured, including those characterized by an entanglement between OAM and polarization. The next step was then to demonstrate a first quantum protocol on such ququarts, that is, the optimal quantum cloning $1 \rightarrow 2$ of ququarts achieved by exploiting the four-dimensional HOM effect [99], as illustrated in figure 12.

The ability to clone a ququart codified in the OAM–polarization space in all the mutually unbiased bases has also been experimentally verified by reconstructing their density matrices through quantum state tomography. The overlap between clones and original quantum state experimentally observed is in good accordance with theoretical predictions involving the increasing dimensionality of the quantum system [105, 90].

An interesting result obtained by working within the SAM–OAM 4D space has been the experimental investigation (not based on the q-plate device) of the topological phase arising in transformations taking place in the space of maximally entangled SAM–OAM states, that provides a representation of the SO(3) group [106]. The SAM–OAM continuous-variable hyper-entanglement has been also demonstrated recently by the same group [107].

In addition to the experimental works discussed above, a number of theoretical works have explored many other

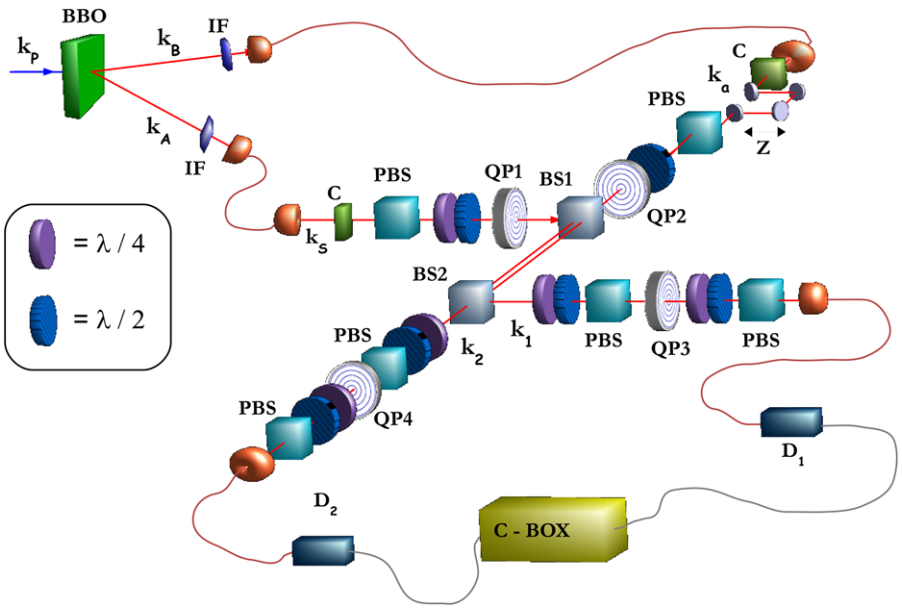

Figure 12. Experimental apparatus for implementing the $1 \rightarrow 2$ optimal quantum cloning of polarization–OAM photon ququarts [99].

possible applications of the q-plate, or more generally of employing an SAM–OAM combination, in the quantum information field. For example, the possibility of using a q-plate for increasing the effective Shannon dimensionality of an entangled pair of photons generated by SPDC, as a consequence of spin–orbit hyper-entanglement, has been proposed [108]. Related works exploiting the combination of SAM and transverse-mode degrees-of-freedom entanglement in SPDC have also been reported, showing also a link with the field of quantum imaging [109]. A three-degrees-of-freedom single photon entanglement, involving SAM, OAM, and optical frequency, can be generated by means of rotating q-plates, thanks to a rotational Doppler shift effect [110]. The implementation of so-called quantum walks in OAM space, or in hybrid SAM–OAM space, has also been investigated very recently [111, 112].

We notice that several single photon quantum information protocols involving SAM–OAM combined manipulations can also be implemented without making recourse to q-plates, by using suitable interferometric layouts in combination with OAM manipulating devices such as spiral phase plates, Dove prisms, cylindrical lenses, etc (see, e.g., [113, 95, 114]). In all these setups, the main working principle is the conversion of the polarization qubit into a path (or 'dual rail') qubit, and vice versa, by means of polarizing beam splitters. Although these approaches are fully appropriate for demonstration purposes, an obvious practical advantage of the q-plate-based setups is that they do not require interferometric stability and may often carry out the entire desired quantum manipulation remaining within a single-beam geometry.

6. Conclusions

In summary, we have surveyed recent progress in the field of the orbital angular momentum of light, with specific attention given to its interaction with the optical spin angular momentum, i.e. the light polarization. The first reported experimental demonstrations of the possibility of interconverting the SAM and OAM of a paraxial light beam and of single photons have stimulated an intense research effort in the last few years. In particular, new methods of generation, control, and manipulation of the optical OAM, both in the classical and quantum regimes, have been demonstrated using the recently introduced device named the q-plate. Such a device is relatively easy to manufacture, and it is tunable and highly efficient. Its action introduces a controlled coupling between polarization (SAM) and OAM that can be conveniently exploited in many different ways. The combination of one or more q-plates and more standard polarization or OAM devices (such as the Dove prism) in suitable schemes allows the achievement of many new optical functionalities. In addition, a number of schemes and experiments not using the q-plate, but still exploiting the SAM and OAM of light and their reciprocal interaction, have recently been reported.

Perhaps the most interesting potential of the combined use of polarization and OAM of light lies in the quantum information field, since the multi-dimensionality of the OAM space provides a natural possibility for implementing qudits within single photons. The hunt for a higher quantum dimensionality of the photon is hence open!

Acknowledgments

We acknowledge the financial support of the Future and Emerging Technologies (FET) programme within the Seventh Framework Programme for Research of the European Commission, under FET-Open grant number 255914- PHORBITECH.

Note added in proof. Another interesting case of optical spin–orbit coupling occurs in the curved spacetime geometry surrounding a rotating black hole, as demonstrated very recently in [115].

References

[1] Humblet J 1943 Sur le moment d'impulsion d'une onde electromagnetique *Physica* **10** 585–603

[2] Franke-Arnold S, Allen L and Padgett M J 2008 Advances in optical angular momentum *Laser Photon. Rev.* **2** 299–313

[3] Van Enk S J and Nienhuis G 1994 Spin and orbital angular momentum of photons *Europhys. Lett.* **25** 497–501

[4] Van Enk S J and Nienhuis G 1994 Commutation rules and eigenvalues of spin and orbital angular momentum of radiation fields *J. Mod. Opt.* **41** 963–77

[5] Barnett S M 2002 Optical angular-momentum flux *J. Opt. B: Quantum Semiclass. Opt.* **4** S7–16

[6] Nieminen T A, Stilgoe A B, Heckenberg N R and Rubinsztein-Dunlop H 2008 Angular momentum of a strongly focused Gaussian beam *J. Opt. A: Pure Appl. Opt.* **10** 115005

[7] Li C-F 2009 Spin and orbital angular momentum of a class of nonparaxial light beams having a globally defined polarization *Phys. Rev.* A **80** 063814

[8] Barnett S M 2010 Rotation of electromagnetic fields and the nature of optical angular momentum *J. Mod. Opt.* **57** 1339–43

[9] Allen L, Beijersbergen M W, Spreeuw R J C and Woerdman J P 1992 Orbital angular momentum of light and the transformation of Laguerre–Gaussian laser modes *Phys. Rev.* A **45** 8185–9

[10] O'Neil A T, MacVicar I, Allen L and Padgett M J 2002 Intrinsic and extrinsic nature of the orbital angular momentum of a light beam *Phys. Rev. Lett.* **88** 053601

[11] He H, Friese M E J, Heckenberg N R and Rubinsztein-Dunlop H 1995 Direct observation of transfer of angular momentum to absorptive particles from a laser beam with a phase singularity *Phys. Rev. Lett.* **75** 826–9

[12] Simpson N B, Dholakia K, Allen L and Padgett M 1997 Mechanical equivalence of spin and orbital angular momentum of light: an optical spanner *Opt. Lett.* **22** 52–4

[13] Piccirillo B and Santamato E 2004 Light angular momentum flux and forces in birefringent inhomogeneous media *Phys. Rev.* E **69** 056613

[14] Beijersbergen M W, Coerwinkel R P C, Kristensen M and Woerdman J P 1994 Helical-wavefront laser beams produced with a spiral phaseplate *Opt. Commun.* **112** 321–7

[15] Bazhenov V Y, Vasnetsov M V and Soskin M S 1990 Laser beams with screw dislocations in their wavefronts *Sov. Phys.—JETP Lett.* **52** 429–31
Bazhenov V Y, Vasnetsov M V and Soskin M S 1990 *Pis. Zh. Eksp. Teor. Fiz.* **52** 1037–9

[16] Bazhenov V Y, Soskin M S and Vasnetsov M V 1992 Screw dislocations in light wavefronts *J. Mod. Opt.* **39** 985–90

[17] Basistiy I V, Bazhenov V Yu, Soskin M S and Vasnetsov M V 1993 Optics of light beams with screw dislocations *Opt. Commun.* **103** 422–8

[18] Leach J, Padgett M J, Barnett S M, Franke-Arnold S and Courtial J 2002 Measuring the orbital angular momentum of a single photon *Phys. Rev. Lett.* **88** 257901

[19] Slussarenko S, D'Ambrosio V, Piccirillo B, Marrucci L and Santamato E 2010 The polarizing sagnac interferometer: a tool for light orbital angular momentum sorting and spin–orbit photon processing *Opt. Express* **18** 27205–16

[20] Bhandari R 1997 Polarization of light and topological phases *Phys. Rep.* **281** 1–64

[21] Biener G, Niv A, Kleiner V and Hasman E 2002 Formation of helical beams by use of Pancharatnam–Berry phase optical elements *Opt. Lett.* **27** 1875–7

[22] Bomzon Z, Biener G, Kleiner V and Hasman E 2002 *Opt. Lett.* **27** 1141–3

[23] Lombard E, Drezet A, Genet C and Ebbesen T W 2010 Polarization control of non-diffractive helical optical beams through subwavelength metallic apertures *New J. Phys.* **12** 023027

[24] Marrucci L, Manzo C and Paparo D 2006 Optical spin-to-orbital angular momentum conversion in inhomogeneous anisotropic media *Phys. Rev. Lett.* **96** 163905

[25] Marrucci L, Manzo C and Paparo D 2006 Pancharatnam–Berry phase optical elements for wavefront shaping in the visible domain: switchable helical modes generation *Appl. Phys. Lett.* **88** 221102

[26] Nagali E, Sciarrino F, De Martini F, Marrucci L, Piccirillo B, Karimi E and Santamato E 2009 Quantum information transfer from spin to orbital angular momentum of photons *Phys. Rev. Lett.* **103** 013601

[27] Abbate G, Maddalena P, Marrucci L, Saetta L and Santamato E 1991 Photodynamical effects induced by the angular momentum of light in liquid crystals *Phys. Scr.* **T39** 389–93

[28] Santamato E, Daino B, Romagnoli M, Settembre M and Shen Y R 1986 Collective rotation of molecules driven by the angular momentum of light in a nematic film *Phys. Rev. Lett.* **57** 2423–6

[29] Marrucci L, Abbate G, Ferraiuolo S, Maddalena P and Santamato E 1992 Self-induced stimulated light scattering in nematic liquid crystals: theory and experiment *Phys. Rev.* A **46** 4859–68

[30] Marrucci L and Paparo D 1997 Photoinduced molecular reorientation of absorbing liquid crystals *Phys. Rev.* E **56** 1765–72

[31] Piccirillo B, Toscano C, Vetrano F and Santamato E 2001 Orbital and spin photon angular momentum transfer in liquid crystals *Phys. Rev. Lett.* **86** 2285–8

[32] Kreuzer M, Benkler E, Paparo D, Casillo G and Marrucci L 2003 Molecular reorientation by photoinduced modulation of rotational mobility *Phys. Rev.* E **68** 011701

[33] Manzo C, Paparo D, Marrucci L and Janossy I 2006 Light-induced rotation of dye-doped liquid crystal droplets *Phys. Rev.* E **73** 051707

[34] Brasselet E, Murazawa N, Misawa H and Juodkazis S 2009 Optical vortices from liquid crystal droplets *Phys. Rev. Lett.* **103** 103903

[35] Jánossy I 2008 Electromagnetic torque and force in axially symmetric liquid-crystal droplets *Opt. Lett.* **33** 2371–3

[36] Marrucci L 2008 Generation of helical modes of light by spin-to-orbital angular momentum conversion in inhomogeneous liquid crystals *Mol. Cryst. Liq. Cryst.* **488** 148–62

[37] Karimi E, Piccirillo B, Marrucci L and Santamato E 2009 Light propagation in a birefringent plate with topological unit charge *Opt. Lett.* **34** 1225–7

[38] Karimi E, Piccirillo B, Nagali E, Marrucci L and Santamato E 2009 Efficient generation and sorting of orbital angular momentum eigenmodes of light by thermally tuned q-plates *Appl. Phys. Lett.* **94** 231124

[39] Stütz M, Gröblacher S, Jennewein T and Zeilinger A 2007 How to create and detect n-dimensional entangled photons with an active phase hologram *Appl. Phys. Lett.* **90** 261114

[40] Straupe S and Kulik S 2010 Quantum optics: the quest for higher dimensionality *Nat. Photon.* **4** 585–6

[41] Ferrari J A, Dultz W, Schmitzer H and Frins E 2007 Achromatic wavefront forming with space-variant polarizers: application to phase singularities and light focusing *Phys. Rev.* A **76** 053815

[42] Chen L X and She W L 2009 Electrically tunable and spin-dependent integer or noninteger orbital angular momentum generator *Opt. Lett.* **34** 178–80

[43] Ciattoni A, Cincotti G and Palma C 2003 Circularly polarized beams and vortex generation in uniaxial media *J. Opt. Soc. Am.* A **20** 163–71

[44] Ciattoni A, Cincotti G and Palma C 2003 Angular momentum dynamics of a paraxial beam in a uniaxial crystal *Phys. Rev.* E **67** 036618

[45] Brasselet E, Izdebskaya Y, Shvedov V, Desyatnikov A S, Krolikowski W and Kivshar Y S 2009 Dynamics of optical spin–orbit coupling in uniaxial crystals *Opt. Lett.* **34** 1021–3

[46] Loussert C and Brasselet E 2010 Efficient scalar and vectorial singular beam shaping using homogeneous anisotropic media *Opt. Lett.* **35** 7–9

[47] Fadeyeva T A, Shvedov V G, Izdebskaya Y V, Volyar A V, Brasselet E, Neshev D N, Desyatnikov A S, Krolikowski W and Kivshar Y S 2010 Spatially engineered polarization states and optical vortices in uniaxial crystals *Opt. Express* **18** 10848–63

[48] Berry M V, Jeffrey M R and Mansuripur M 2005 Orbital and spin angular momentum in conical diffraction *J. Opt. A: Pure Appl. Opt.* **7** 685–90

[49] O'Dwyer D P, Phelan C F, Rakovich Y P, Eastham P R, Lunney J G and Donegan J F 2010 Generation of continuously tunable fractional optical orbital angular momentum using internal conical diffraction *Opt. Express* **18** 16480–5

[50] Zhao Y, Edgar J S, Jeffries G D M, McGloin D and Chiu D T 2007 Spin-to-orbital angular momentum conversion in a strongly focused optical beam *Phys. Rev. Lett.* **99** 073901

[51] Adachi H, Akahoshi S and Miyakawa K 2007 Orbital motion of spherical microparticles trapped in diffraction patterns of circularly polarized light *Phys. Rev.* A **75** 063409

[52] Chen L X and She W L 2008 Electro-optic ally forbidden or enhanced spin-to-orbital angular momentum conversion in a focused light beam *Opt. Lett.* **33** 696–8

[53] Wang X-L, Chen J, Li Y, Ding J, Guo C-S and Wang H-T 2010 Optical orbital angular momentum from the curl of polarization *Phys. Rev. Lett.* **105** 253602

[54] Onoda M, Murakami S and Nagaosa N 2004 Hall effect of light *Phys. Rev. Lett.* **93** 083901

[55] Hosten O and Kwiat P 2008 Observation of the spin Hall effect of light via weak measurements *Science* **319** 787–90

[56] Bliokh K Y, Niv A, Kleiner V and Hasman E 2008 Geometrodynamics of spinning light *Nat. Photon.* **2** 748–53

[57] Bliokh K Y 2009 Geometrodynamics of polarized light: Berry phase and spin Hall effect in a gradient-index medium *J. Opt. A: Pure Appl. Opt.* **11** 094009

[58] Rodríguez-Herrera O G, Lara D, Bliokh K Y, Ostrovskaya E A and Dainty C 2010 Optical nanoprobing via spin–orbit interaction of light *Phys. Rev. Lett.* **104** 253601

[59] Soskin M S and Vasnetsov M V 2001 Singular optics *Prog. Opt.* **42** 219–76

[60] Soskin M S, Denisenko V and Freund I 2003 Optical polarization singularities and elliptic stationary points *Opt. Lett.* **28** 1475–7

[61] Dennis M R, O'Holleran K and Padgett M J 2009 Singular optics: optical vortices and polarization singularities *Prog. Opt.* **53** 293–364

[62] Freund I 2010 Multitwist optical Möbius strips *Opt. Lett.* **35** 148–50

[63] Sanvitto D *et al* 2010 Persistent currents and quantized vortices in a polariton superfluid *Nat. Phys.* **6** 527–33

[64] Shelykh I A, Kavokin A V, Rubo Y G, Liew T C H and Malpuech G 2010 Polariton polarization-sensitive phenomena in planar semiconductor microcavities *Semicond. Sci. Technol.* **25** 013001

[65] Nersisyan S, Tabiryan N, Steeves D M and Kimball B R 2009 *Opt. Express* **17** 11926

[66] Slussarenko S, Murauski A, Du T, Chigrinov V, Marrucci L and Santamato E 2011 Tunable liquid crystal q-plates with arbitrary topological charge *Opt. Express* **19** 4085–90

[67] Piccirillo B, D'Ambrosio V, Slussarenko S, Marrucci L and Santamato E 2010 Photon spin-to-orbital angular momentum conversion via an electrically tunable q-plate *Appl. Phys. Lett.* **97** 241104

[68] Mosca S, Canuel B, Karimi E, Piccirillo B, Marrucci L, De Rosa R, Genin E, Milano L and Santamato E 2010 Photon self-induced spin-to-orbital conversion in a terbium–gallium–garnet crystal at high laser power *Phys. Rev.* A **82** 043806

[69] Morikawa J, Orie A, Hashimoto T and Juodkazis S 2010 Thermal and optical properties of the femtosecond-laser-structured and stress-induced birefringent regions in sapphire *Opt. Express* **18** 8300–10

[70] Brasselet E 2009 Singular optical manipulation of birefringent elastic media using nonsingular beams *Opt. Lett.* **34** 3229–31

[71] Brasselet E 2010 Spin–orbit optical cross-phase-modulation *Phys. Rev.* A **82** 063836

[72] Calvó G F and Picon A 2007 Spin-induced angular momentum switching *Opt. Lett.* **32** 838–40

[73] Karimi E, Zito G, Piccirillo B, Marrucci L and Santamato E 2007 Hypergeometric-Gaussian modes *Opt. Lett.* **32** 3053–5

[74] Vaveliuk P 2009 Nondiffracting wave properties in radially and azimuthally symmetric optical axis phase plates *Opt. Lett.* **34** 3641–3

[75] Carvalho A M de M, Sátiro C and Moraes F 2007 Aharonov-bohm like effect for light propagating in nematics with disclinations *Europhys. Lett.* **80** 46002

[76] Padgett M J and Courtial J 1999 Poincaré-sphere equivalent for light beams containing orbital angular momentum *Opt. Lett.* **24** 430–2

[77] Nagali E, Sciarrino F, De Martini F, Piccirillo B, Karimi E, Marrucci L and Santamato E 2009 Polarization control of single photon quantum orbital angular momentum states *Opt. Express* **17** 18745–59

[78] Karimi E, Slussarenko S, Piccirillo B, Marrucci L and Santamato E 2010 Polarization-controlled evolution of light transverse modes and associated Pancharatnam geometric phase in orbital angular momentum *Phys. Rev.* A **81** 053813

[79] Coutinho dos Santos B, Souza C E R, Dechoum K and Khoury A Z 2007 Phase conjugation and adiabatic mode conversion in a driven optical parametric oscillator with orbital angular momentum *Phys. Rev.* A **76** 053821

[80] Slussarenko S, Karimi E, Piccirillo B, Marrucci L and Santamato E 2011 Efficient generation and control of different-order orbital angular momentum states for communication links *J. Opt. Soc. Am.* A **28** 61–5

[81] Slussarenko S, Karimi E, Piccirillo B, Marrucci L and Santamato E 2009 Universal unitary gate for single-photon spin–orbit four-dimensional states *Phys. Rev.* A **80** 022326

[82] De Martini F and Sciarrino F 2005 Non-linear parametric processes in quantum information *Prog. Quantum Electron.* **29** 165–256

[83] Molina-Terriza G, Torres J P and Torner L 2007 Twisted photons *Nat. Phys.* **3** 305–10

[84] Barreiro J T, Langford N K, Peters N A and Kwiat P G 2005 Generation of hyperentangled photon pairs *Phys. Rev. Lett.* **95** 260501

[85] Barreiro J T, Wei T-C and Kwiat P G 2008 Beating the channel capacity limit for linear photonic superdense coding *Nat. Phys.* **4** 282–6

[86] Aolita L and Walborn S P 2007 Quantum communication without alignment using multiple-qubit single-photon states *Phys. Rev. Lett.* **98** 100501

[87] Souza C E R, Borges C V S, Khoury A Z, Huguenin J A O, Aolita L and Walborn S P 2008 Quantum key distribution without a shared reference frame *Phys. Rev.* A **77** 032345

[88] Marrucci L, Nagali E, Sciarrino F, Sansoni L, De Martini F, Piccirillo B, Karimi E and Santamato E 2010 Photonic quantum information applications of patterned liquid crystals *Mol. Cryst. Liq. Cryst.* **526** 108–18

[89] Hong C K, Ou Z Y and Mandel L 1987 Measurement of subpicosecond time intervals between two photons by interference *Phys. Rev. Lett.* **59** 2044–6

[90] Nagali E, Sansoni L, Sciarrino F, De Martini F, Marrucci L, Piccirillo B, Karimi E and Santamato E 2009 Optimal quantum cloning of orbital angular momentum photon qubits through Hong–Ou–Mandel coalescence *Nat. Photon.* **3** 720–3

[91] Nagali E and Sciarrino F 2010 Generation of hybrid polarization-orbital angular momentum entangled states *Opt. Express* **18** 18243–8

[92] Karimi E, Leach J, Slussarenko S, Piccirillo B, Marrucci L, Chen L, She W, Franke-Arnold S, Padgett M J and Santamato E 2010 Spin–orbit hybrid entanglement of photons and quantum contextuality *Phys. Rev.* A **82** 022115

[93] Mair A, Vaziri A, Welhs G and Zeilinger A 2001 Entanglement of the angular momentum states of photons *Nature* **412** 313–6

[94] Chen L X and She W L 2010 Single-photon spin–orbit entanglement violating a Bell-like inequality *J. Opt. Soc. Am.* B **27** A7–10

[95] Borges C V S, Hor-Meyll M, Huguenin J A O and Khoury A Z 2010 Bell-like inequality for the spin–orbit separability of a laser beam *Phys. Rev.* A **82** 033833

[96] Chen L X and She W L 2009 Teleportation of a controllable orbital angular momentum generator *Phys. Rev.* A **80** 063831

[97] Barreiro J T, Wei T-C and Kwiat P G 2010 Remote preparation of single-photon hybrid entangled and vector-polarization states *Phys. Rev. Lett.* **105** 030407

[98] Chen L X and She W L 2011 Hybrid entanglement swapping of photons: creating the orbital angular momentum bell states and Greenberger–Horne–Zeilinger states *Phys. Rev.* A **83** 012306

[99] Nagali E, Giovannini D, Marrucci L, Slussarenko S, Santamato E and Sciarrino F 2010 Experimental optimal cloning of four-dimensional quantum states of photons *Phys. Rev. Lett.* **105** 073602

[100] Moreva E V, Maslennikov G A, Straupe S S and Kulik S P 2006 Realization of four-level qudits using biphotons *Phys. Rev. Lett.* **97** 023602

[101] Bogdanov Yu I, Moreva E V, Maslennikov G A, Galeev R F, Straupe S S and Kulik S P 2006 Polarization states of four-dimensional systems based on biphotons *Phys. Rev.* A **73** 063810

[102] Vallone G, Pomarico E, De Martini F, Mataloni P and Barbieri M 2007 Experimental realization of polarization qutrits from nonmaximally entangled states *Phys. Rev.* A **76** 012319

[103] Baek S-Y and Kim Y-H 2007 Generating entangled states of two ququarts using linear optical elements *Phys. Rev.* A **75** 034309

[104] Nagali E, Sansoni L, Marrucci L, Santamato E and Sciarrino F 2010 Experimental generation and characterization of single-photon hybrid ququarts based on polarization and orbital angular momentum encoding *Phys. Rev.* A **81** 052317

[105] Bruß D, DiVincenzo D P, Ekert A, Fuchs C A, Macchiavello C and Smolin J A 1998 Optimal universal and state-dependent quantum cloning *Phys. Rev.* A **57** 2368–78

[106] Souza C E R, Huguenin J A O, Milman P and Khoury A Z 2007 Topological phase for spin–orbit transformations on a laser beam *Phys. Rev. Lett.* **99** 160401

[107] Coutinho dos Santos B, Dechoum K and Khoury A Z 2009 Continuous-variable hyperentanglement in a parametric oscillator with orbital angular momentum *Phys. Rev. Lett.* **103** 230503

[108] Chen L X and She W L 2009 Increasing shannon dimensionality by hyperentanglement of spin and fractional orbital angular momentum *Opt. Lett.* **34** 1855–7

[109] Caetano D P, Souto Ribeiro P H, Pardal J T C and Khoury A Z 2003 Quantum image control through polarization entanglement in parametric down-conversion *Phys. Rev.* A **68** 023805

[110] Chen L X and She W L 2008 Sorting photons of different rotational doppler shifts (rds) by orbital angular momentum of single-photon with spin–orbit-rds entanglement *Opt. Express* **16** 14629–34

[111] Zhang P, Liu B-H, Liu R-F, Li H-R, Li F-L and Guo G-C 2010 Implementation of one-dimensional quantum walks on spin–orbital angular momentum space of photons *Phys. Rev.* A **81** 052322

[112] Hamilton C S, Gábris A, Jex I and Barnett S M 2011 Quantum walk with a four-dimensional coin *New J. Phys.* **13** 013015

[113] Chen L X and She W L 2009 Encoding orbital angular momentum onto multiple spin states based on a Huffman tree *New J. Phys.* **11** 103002

[114] Souza C E R and Khoury A Z 2010 A michelson controlled-not gate with a single-lens astigmatic mode converter *Opt. Express* **18** 9207–12

[115] Tamburrini F, Thide B, Molina-Terriza G and Anzolin G 2011 Twisting of light around rotating black holes *Nature Phys.* **7** 195–7